Improved Response Functions For The MicroSkyshine Method

by

J. K. Shultis and R. E. Faw

Nuclear Engineering Department
Kansas State University
Manhattan, KS 66506

May 1987

Kansas State University
College of Engineering
Engineering Experiment Station

Report 189

TABLE OF CONTENTS

		Page
1.	Summary	1
2.	Introduction	2
	2.1 Need for Improvement in Response Functions	2
	2.2 Need for Angular Interpolation	3
	2.3 Scope of Report	4
3.	Revised Beam Response Functions	6
	3.1 Calculation of Skyshine from a Gamma-Photon Beam	6
	3.2 Approximation to the Beam Response Functions	10
	3.3 Interpolation of the Response Functions	12
4.	Results Obtained with Improved Response Functions	16
	4.1 Comparison of Old and New Response Functions	16
	4.2 Comparison with Monte Carlo Calculations	17
	4.3 Comparison with Moments-Method Calculations	18
	4.4 Skyshine Benchmark Calculations	19
	4.4.1 ANSI/ANS-6.6.1 Reference Problems	19
	4.4.2 Methods Used for Reference Calculations	21
	4.4.3 Comparison of Results for ANSI Problem I.1	22
	4.4.4 Comparison of Results for ANSI Problem I.2	23
	4.5 Comparison to Moments Methods	23
	4.5.1 Description of Experiments	23
	4.5.2 Experimental Results	24
	4.5.3 Comparison of Calculated and Measured Results	25
	4.5.4 Comparison with Hybrid ANISN/SKYSHINE-II Calculations	26
5.	Bibliography	38
APPENDIX A:	Coefficients for the Improved Line-Beam Gamma-Ray Response Functions	
APPENDIX B:	Gamma-Ray Mass Interaction Coefficients Used in the Improved MicroSkyshine Method	
APPENDIX C:	Coefficients for Air-Kerma (Exposure) Buildup Factors Used in Generating Line-Beam Response Functions	

1. Summary

A new set of response function is presented for use in the *MicroSkyshine* method for gamma-ray skyshine calculations.* This method, described in an earlier report [Fa87], uses so-called line-beam response functions to evaluate the air-scattered (skyshine) dose rate resulting from a point isotropic and monoenergetic source occluded from the detector by an intervening silo or plane wall. Specifically, a point-kernel technique is used to computed the response functions for 12 source energies and 20 beam directions. The new response functions avoid minor problems incurred with the utilization of Monte Carlo based response functions in the *MicroSkyshine* method.

To the newly calculated beam response functions, a simple three-parameter function is least-squares fit and a set of response function coefficients is obtained which allow accurate evaluation of the response function for energies between 0.1 and 10 MeV and for beam directions up to 180 degrees. To make the beam functions that are reconstituted from the new set of coefficients continuous in both energy and angle, a linear interpolation scheme is presented.

Finally, comparison calculations are presented. With the new continuous response functions, artificially induced inconsistencies resulting from interpolation within the discrete (histogram) form of the earlier response functions are now eliminated. From comparisons to benchmark measurements and calculations, it is shown that the new set of response-function coefficients allows skyshine calculations to be made over a greater source-to-detector distance and to give results that are more accurate than those based on the original coefficients.

---

*All distributed copies of the *MicroSkyshine* code [Gr87] employ the new response functions.

2. Introduction

In an earlier report [Fa87] a methodology was presented for the calculation of skyshine radiation originating from a point source occluded from a detector by a concentric annular silo or an intervening plane wall. This method, which is implemented in the recent microcomputer code *MicroSkyshine* [Gr87], is based on so-called line-beam response functions. These functions give the absorbed dose rate in air as a function of distance from a point monodirectional source emitting monoenergetic photons at angles up to 180 degrees from the source-detector axis. With these beam response functions, the *MicroSkyshine* method decomposes the angularly distributed photons emitted skyward into a series of line beams and integrates (sums) over all beam directions permitted by the geometry of the problem to obtain the dose rate at a specified detector location. The use of line-beam response functions thus makes an inherently difficult radiation transport problem amenable to rapid calculation by microcomputer.

The line-beam response functions used in the initial development of the *MicroSkyshine* method were obtained by Radiation Research Associates (RRA) by fitting an empirical function with three adjustable parameters to results of Monte Carlo calculations. These beam functions then formed the basis of the SKYSHINE and SKYSHINE-II codes [Pr76, La79], and were incorporated successfully into the *MicroSkyshine* microcomputer program [Fa87].

2.1 Need for Improvement in Response Functions

While the original RRA response functions gave satisfactory results for most skyshine problems [Fa87], small sporadic discontinuities can

observed in the parameters of the beam response functions for neighboring energy or angular groups. That such errors should be present in the tabulated coefficients is not surprising since the coefficients were obtained by fits to Monte Carlo data which themselves must have contained statistical errors. These fitting errors are manifested as spurious dips in the energy response of the calculated skyshine doses (particularly around 5-6 MeV, an energy region of importance for ^{16}N skyshine problems).

Of greater concern are inadequacies in the beam response functions for very large source-to-detector distances. The use of the original RRA beam response functions in *MicroSkyshine* yielded good agreement with measurements and benchmark calculations over the 1500-m source-to-detector range used for fitting the response functions. However, the calculated skyshine dose rates at distances from the source approaching this limit not only were somewhat conservative (overpredictive) but did not decrease as rapidly with increasing distance from the source as did other results. This asymptotic behavior precluded extrapolation of results beyond the 1500m limit of the response functions, since such an extrapolation would predict far too large a skyshine dose.

Finally, another minor deficiency in the RRA response functions was apparent for photons with energies above 9.5 MeV. For such photons, an extrapolation of the beam functions at 8.5 and 9.5 MeV was made by *MicroSkyshine*, and, for source-to-detector distances much greater than 1000 m, the extrapolated skyshine dose rates were negative for certain beam directions. These negative extrapolated values arise from relatively large differences in the RRA 8.5 and 9.5 MeV response functions. In reality, the skyshine dose should vary but little over this energy range.

2.2 Need for Angular Interpolation

In the *MicroSkyshine* development, the line-beam response functions were linearly interpolated between adjacent energy groups to give a continuous variation of skyshine doses with photon energy. The

variation with the angle between the source ray and the source-detector axis, however, was left as a discrete histogram based on the 20 angular groups of the RRA response functions. This treatment of the angular variable, while not producing significant errors in calculated dose rates for an angularly distributed source, did occasionally produce small (a few percent) random variations in the calculated doses when one of the geometry parameters was altered slightly. These random variations could be observed for tightly collimated skyshine sources and, equivalently, for sources which were shielded above by thick plane shields.

Such random variations in the calculated skyshine doses make sensitivity studies difficult since rather large parameter changes must be used to obtain changes in the dose which are substantially greater than the random variations resulting from the lack of angular continuity for the response functions. The use of line-beam response functions which vary continuously in angle would eliminate this deficiency.

2.4 Scope of Report

The purpose of this report is to present methods for correcting the above two deficiencies in the *MicroSkyshine* method as originally reported by Faw and Shultis [FaS7]. Specifically, a method for calculating more suitable line-beam response functions is presented and an alternative set of response function coefficients is given. Besides better predicting asymptotic behavior of skyshine dose rates, this new set of response-function coefficients also eliminates spurious fluctuations between neighboring coefficients. As a result, the new coefficients appear to extend the source-to-detector range over which the *MicroSkyshine* method can be applied.

A second topic of this report is the introduction of an interpolation scheme to make the angular variation of the response function continuous and thereby to eliminate the small random fluctuations in computed skyshine doses. While this interpolation

A second topic of this report is the introduction of an interpolation scheme to make the angular variation of the response function continuous and thereby to eliminate the small random fluctuations in computed skyshine doses. While this interpolation scheme improves the precision of the skyshine calculations, it has little effect on their accuracy. However, with this scheme, sensitivity studies are now more easily performed.

Finally, comparisons of results obtained with the new response functions to measurements and benchmark calculations are presented. From these comparisons, it is seen that the new line-beam response functions produce more accurate results, particularly at large distances from the source.

3. Revised Beam Response Functions

In this chapter a method is presented for the evaluation of the dose rate arising from a monodirectional, monoenergetic beam of photons emitted at angle ϕ to the source-detector axis. From results of this method, an analytical function with three parameters is fit and a set of parameter values is presented which can then be used to reconstitute the line-beam response functions needed by the *MicroSkyshine* method. With the new beam response functions derived here, more accurate skyshine dose rates over a greater source-to-detector range can be obtained. Finally, to make the beam response functions continuous in angle, an angular interpolation scheme is presented.

3.1 Calculation of Skyshine from a Gamma-Photon Beam

Consider a point monoenergetic photon source which is in an infinite homogeneous air medium and which emits photons of energy E in a direction ϕ from the axis between the source and a point detector which is distance x away (see Fig. 3.1). Many techniques may be used to calculate the dose rate at the detector. In obtaining the RRA line-beam response functions [La79], the Monte Carlo method was used. That method, however, is computationally intensive particularly for large source distances x. Similarly, discrete-ordinates transport methods are also difficult to apply since the problem is inherently multi-dimensional.

As an alternative, albeit approximate, method, the point kernel technique can be employed to evaluate the dose per photon at the detector. The probability a source photon travels a distance y along

the beam and then, while traversing dy, scatters through an angle θ_s into a unit solid angle is

$$N\ Z\ {}_e\sigma_s(E,\theta_s)\ e^{-\mu y}\ dy$$

where N is the atomic density of the air, Z is the average number of electrons per air atom (7.225), μ is the total linear interaction coefficient for photons of energy E, and ${}_e\sigma_s(E,\theta_s)$ is the microscopic differential scattering cross section per electron for photons of energy E scattering into unit solid angle through a scattering angle θ_s (E' is the energy of the scattered photon). If E > 1.02 MeV, annihilation photons (energy E_a = 0.511 MeV) may also be generated as a result of pair production interactions in dy. If the distance traveled by the positron is neglected, the probability a source photon will produce in dy an annihilation photon in a unit solid angle directed towards the detector is

$$\frac{1}{2\pi}\ N\ \sigma_{pp}(E)\ e^{-\mu y}\ dy,$$

where σ_{pp} is the microscopic pair-production cross section (per atom).

To account for the buildup of secondary photons as the photons produced in dy travel a distance r to the detector, multiply the uncollided dose (from photons originating in dy) by an appropriate buildup factor B. Then to obtain the total dose at the detector simply integrate over all dy along the beam. Thus the total dose per photon at the detector is

$$\mathcal{H}(E,x,\phi) = N \int_0^\infty \frac{\exp(-\mu y)}{r^2} \left[Z\ {}_e\sigma_s\ \exp(-\mu' r)\ B(E',\mu' r)\ \mathcal{H}(E') \right.$$

$$\left. +\ \frac{\sigma_{pp}}{2\pi}\ \exp(-\mu_a r)\ B(E_a,\mu_a r)\ \mathcal{H}(E_a) \right] dy \qquad (3.1)$$

where $r^2 = y^2 + x^2 - 2yx\cos\phi$, μ_a is the total linear interaction coefficient for photons of energy E_a, and $\mathcal{K}(E)$ is the detector response function (here the air absorbed dose per unit fluence of photons of energy E). To simplify the numerical evaluation of this result, express distances in mean-free-path lengths. Thus let $\xi = \mu y$, $r' = \mu' r$, $r'' = \mu_a r$, and $R = \mu r$. Then Eq. (3.1) may be written as

$$\mathcal{K}(E,x,\phi) = \rho^2 (\mu/\rho) \int_0^\infty \frac{e^{-\xi}}{R^2} \left[(Z/A) N_a {}_e\sigma_c(E,\theta_s)\, e^{-r'} B(E',r')\, \mathcal{K}(E') \right.$$

$$\left. + \frac{1}{2\pi} (\mu/\rho)_{pp}\, e^{-r''} B(E_a,r'')\, \mathcal{K}(E_a) \right] d\xi. \qquad (3.2)$$

where $R^2 = \xi^2 + \mu^2 x^2 - 2\xi\mu x\cos\phi$, (μ/ρ) is the total mass interaction coefficient in air for photon energy E, $(\mu/\rho)_{pp}$ is the pair-production mass interaction coefficient in air for photon energy E, (Z/A) the charge to mass ratio for air, and ρ is the mass density of air.

To evaluate the integrand of Eq. (3.2), total interaction coefficient data were taken Hubbell [Hu82] and pair-production interaction coefficient data were taken from Storm and Israel [St67]. Tabulated values were logarithmically interpolated to give coefficients at any photon energy. The Klein-Nishina free-electron model was used for the differential scattering cross section, namely [Ch84]

$${}_e\sigma_s(E,\theta_s) = r_e^2 (E'/E)\{1 + (E'/E)^2 - (E'/E)(1 - \cos^2\theta_s)\}/2, \qquad (3.3)$$

where r_e is the classical electron radius (2.8179×10^{-15} m) and E' is the energy of the scattered photon, given by the Compton formula

$$E' = \frac{E}{1 + (E/E_a)(1 - \cos\theta_s)}. \qquad (3.4)$$

with

$$\cos\theta_s = (x^2 - r^2 - y^2)/2yr = (\mu^2x^2 - R^2 - \xi^2)/2\xi R \ .$$

Finally, the buildup factor B was taken as the exposure (air kerma) buildup factor for a point isotropic source. This buildup factor can be approximated very accurately as [Ha83,Ha86]

$$B(E,X) \simeq \begin{cases} 1 + (b-1)\,\dfrac{(K^X - 1)}{K - 1}\ , & \text{for } K \neq 1 \\ 1 + (b-1)X\ , & \text{for } K = 1 \end{cases} \qquad (3.5)$$

where $X = \mu x$ is the distance from the source in mean-free-path lengths, and K is computed from

$$K(X) = cX^a + d\,\frac{[\tanh(X/X_k - 2) - \tanh(-2)]}{[1 - \tanh(-2)]} \qquad (3.6)$$

The fit parameters a, b, c, d, and X_k in this approximation are taken from a recent revision of the QAD code [Rs86]. (See Appendix C.)

Once the integrand of Eq. (3.2) is evaluated, numerical quadrature can be used to evaluate the integral. In this study, 16-point Gaussian quadrature was used to evaluate each mean-free-path segment of the integral starting from the source and proceeding outward along the beam until either the change in the cumulative integral or the value in relation to that from the preceding segment was less than some small prescribed value. In this manner, skyshine doses were calculated for detector distances up to 5000 m from the source and for beam angles up to 180 degrees.

The above method for evaluating the line-beam response functions, $\mathcal{R}(E,x,\phi)$, involves two approximations. The Klein-Nishina cross section ignores electron binding effects. However, the error introduced by this idealistic cross section is generally small, particularly for the energies considered here, and this approximation is widely used. Of more concern is the use of buildup factors derived for isotropic point

sources. The photons scattering out of dy in the beam are not scattered isotropically but rather are scattered preferentially forward. The use of isotropic buildup factors should thus tend to be conservative by overpredicting the skyshine doses; however, the excellent agreement between the resulting response functions and benchmark measurements and calculations indicates that any error introduced by this approximation must be very small.

3.2 Approximations to the Beam Response Functions

To use the line-beam response functions in the *MicroSkyshine* method, it is necessary to approximate them by a simple analytical expression with a few adjustable parameters. The approximating function introduced by RRA [La79] and adopted in this study is

$$\mathcal{R}(E,x,\phi) = E\ \mathcal{I}(E,x,\phi) \tag{3.7}$$

where

$$\mathcal{I}(E,x,\phi) = \kappa\ (\rho/\rho_o)^2\ [x(\rho/\rho_o)]^b\ \exp[a - cx(\rho/\rho_o)]. \tag{3.8}$$

The parameters a, b, and c are functions of the source energy E and beam angle ϕ, and ρ is the air density in the same units as the reference density ρ_o (0.001225 g/cm^3).

The above expressions are dimensional with E being in units of MeV per photon. For x measured in meters, the fitted expression $x^b e^{a-cx}$ is in units of MeV absorbed per m^3 of air of reference density per MeV of source photon energy. The constant κ is thus equal to $(1.602\times10^{-6}$ erg/MeV)/[(100 erg/g rad)(1225 g/m^3)] = 1.308×10^{-11} rad m^3/MeV. With these units, $\mathcal{I}$ thus has units of rad/MeV and $\mathcal{R}$ rad/photon.

To obtain values for a, b and c, it is necessary to fit Eq. (3.7) to calculated values of the beam skyshine dose $\mathcal{R}(E_i,x,\phi_j)$ for a fixed source energy E_i and beam angle ϕ_j over some range of x. Twelve discrete energies E_i and 20 discrete beam angles ϕ_j were used in this

study. The discrete energies, shown in Table 3.1, are the same as median group energies used in the RRA response functions except for the two lowest energies. The discrete angles are listed in Table 3.2 and are the same as the medians of the angular groups used in the RRA response functions.

Since the beam dose rate $\Re(E,x,\phi)$ varies over many orders of magnitude as x varies over many hundreds of meters, it is preferable to obtain a, b and c by fitting the logarithms of the skyshine doses. Thus for a fixed energy E_i and fixed beam angle ϕ_j, the least squares estimators of a, b and c are those parameter values which minimize

$$S(a,b,c) = \sum_{m=1}^{M} [(G + b\ln x_m + a - cx_m) - \Re_m]^2 \qquad (3.9)$$

where $G = \ln(Ek)$ and $\Re_m = \Re(E_i,x_m,\phi_j)$, m=1...M are the beam doses for various detector distances x_m. The minimum of S is readily found by standard minimization techniques such as the simplex method [Ko68].

To generate a new set of line-beam response coefficients, doses (per photon) were calculated by the method of Section 3.1 for various detector distances at one mean-free-path increments from the source for each energy and angle in Tables 3.1 and 3.2, respectively. For each given energy and angle, the coefficients were found by fitting the calculated dose rates out to at least 2500 m from the source by the above least squares procedure. The results of these fits are presented in Appendix A together with the average percent absolute deviation of the fit to the calculated doses (MAD) and the maximum absolute deviation. The poorest agreement between the fitted response function and the calculated doses almost always occurs when the detector is closest to the source. To be noted is the smooth variation of the coefficients between adjacent angles or energies, a result which eliminates the spurious fluctuations in the original RRA response functions.

3.3 Interpolation of the Response Functions

In the SKYSHINE-II code [La79], a strict multigroup approach for both energy and angle is used to evaluate response functions. However, in the *MicroSkyshine* code, an interpolation procedure is used to make the line-beam response function continuously variable in both energy and angle.

In *MicroSkyshine*, the line-beam response functions are first linearly interpolated in energy to yield the response functions for the energy E of interest at each of the 20 discrete beam directions ϕ_j. If $E_i \leq E \leq E_{i+1}$ then the response functions at these two closest discrete energies are reconstituted from the fit coefficients by Eq. (3.8). If these reconstituted response functions are denoted by

$$\mathcal{F}_{i,j}(x) \equiv \mathcal{F}(E_i,\phi_j,x) \quad \text{and} \quad \mathcal{F}_{i+1,j}(x) \equiv \mathcal{F}(E_{i+1},\phi_j,x) \tag{3.10}$$

then the response function at energy E is given by

$$\mathcal{F}(E,\phi_j,x) = \mathcal{F}_{i+1,j}(x)\,\frac{E_i - E}{E_i - E_{i+1}} + \mathcal{F}_{i,j}(x)\,\frac{E - E_{i+1}}{E_i - E_{i+1}}\,. \tag{3.11}$$

For the last half of the highest energy group, $9.5 < E \leq 10$ MeV, an extrapolation procedure is used, namely

$$\mathcal{F}(E,\phi_j,x) = \mathcal{F}_{1,j}(x)\ (E-8.5) + \mathcal{F}_{2,j}(x)\ (9.5-E)\,. \tag{3.12}$$

Once the interpolation in energy has been performed at all angles ϕ_j, $j = 1,2,\ldots,20$, an interpolation in the beam angle is made. Such an angular interpolation avoids the small random fluctuations in the estimated skyshine doses arising from a Gaussian numerical integration of an integrand which is a histogram in angle. Thus for a beam direction ϕ where $\phi_j \leq \phi \leq \phi_{j+1}$, the response function is estimated as

$$\mathcal{F}(E,\phi,x) = \mathcal{F}(E,\phi_j,x) + \frac{\mathcal{F}(E,\phi_{j+1},x) - F(E,\phi_j,x)}{\phi_{j+1} - \phi_j} \{\phi - \phi_{j+1}\} \ . \quad (3.13)$$

For the intervals (0 - 0.5 degrees) and (170 - 180 degrees) an extrapolation procedure is used; namely, for $0 \leq \phi \leq 0.5 = \phi_1$ degrees

$$\mathcal{F}(E,\phi,x) = \mathcal{F}(E,\phi_1,x) + \frac{\mathcal{F}(E,\phi_2,x) - \mathcal{F}(E,\phi_1,x)}{\phi_2 - \phi_1} \{\phi - \phi_2\} \quad (3.14)$$

and for $\phi_{20} = 170 \leq \phi \leq 180$ degrees

$$\mathcal{F}(E,\phi,x) = \mathcal{F}(E,\phi_{20},x) + \frac{\mathcal{F}(E,\phi_{19},x) - \mathcal{F}(E,\phi_{20},x)}{\phi_{19} - \phi_{20}} \{\phi - \phi_{19}\} \ . \quad (3.15)$$

By this double interpolation scheme, the line-beam response function is rendered continuous in both energy and direction, and *MicroSkyshine* calculated doses will now vary smoothly with small changes in the problem parameters thereby facilitating sensitivity studies. However, it should be noted that while this continuity feature increases the precision of the skyshine calculations, it does require more computational effort and has little effect on the accuracy of the skyshine doses.

Table 3.1

Discrete energy structure used in the definition of the new response functions. Except for the two lowest energies, these energies are the medians of the energy groups used in the RRA response functions.

i	E_i (MeV)
1	9.5
2	8.5
3	7.5
4	6.5
5	5.5
6	4.5
7	3.5
8	2.5
9	1.5
10	0.75
11	~~0.30~~ 0.325
12	~~0.055~~ 0.1

Table 3.2

Discrete beam directions used in the definition of the new response functions. These angles are the medians of the angular groups used in the original RRA response functions.

j	ϕ_j (deg)
1	0.5
2	1.5
3	2.5
4	4.0
5	6.0
6	8.5
7	12.5
8	17.5
9	25.0
10	35.0
11	45.0
12	55.0
13	65.0
14	75.0
15	85.0
16	95.0
17	110.
18	130.
19	150.
20	170.

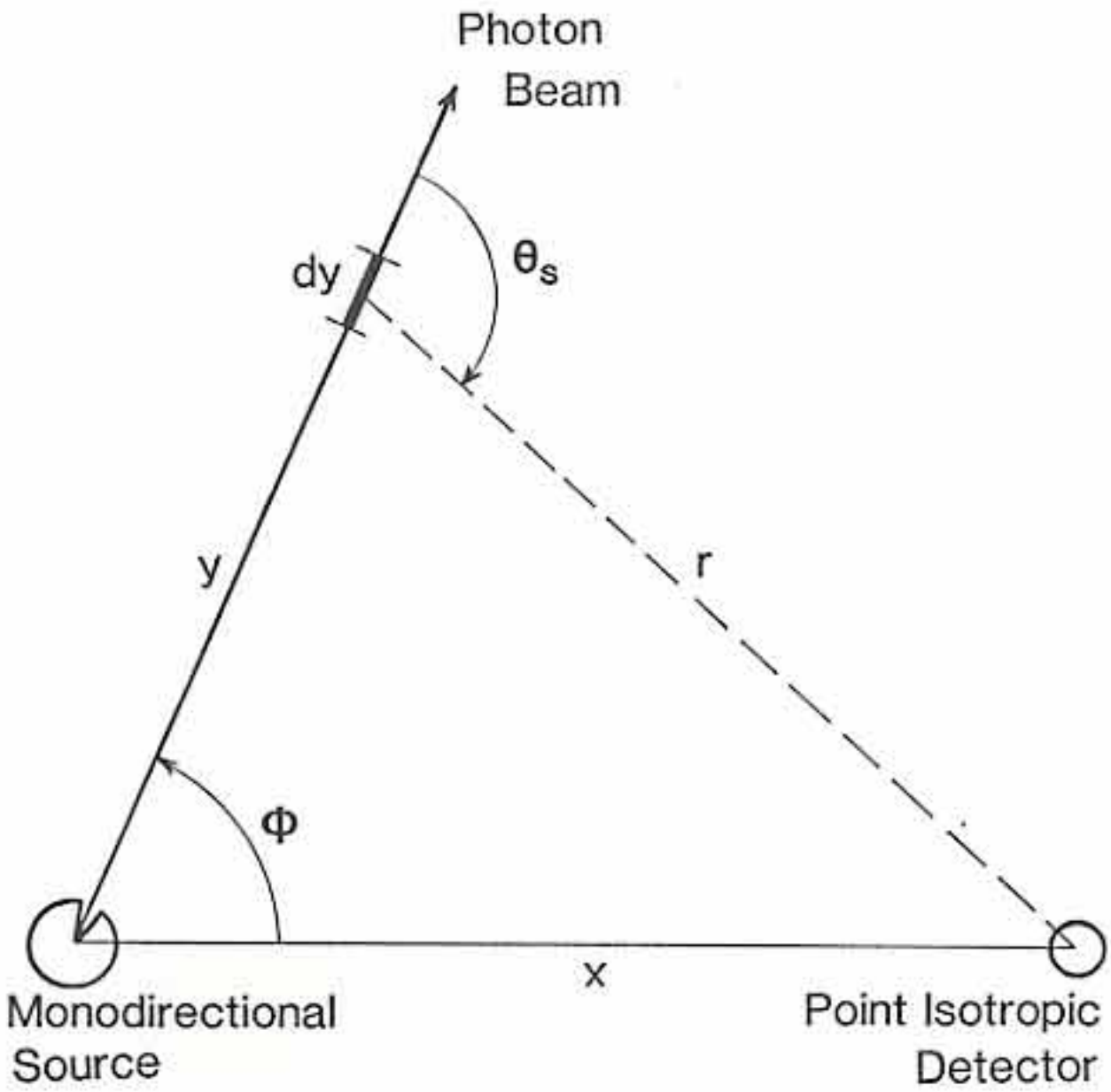

Fig. 3.1 Geometry for calculation of line-beam response functions.

4. Results Obtained With Improved Response Functions

4.1 Comparison of Old and New Response Functions

Unlike the original line-beam response functions $\mathcal{R}(E,\phi,x)$ developed by RRA [La79] which were histograms in both energy and angle, the new response functions proposed here are rendered continuous in both energy and angle by means of linear interpolation between tabulated values. In Fig. 4.1 representative response functions are compared for three differnt energies at a fixed source-to-detector distance as the emission angle varied from 0 to 90 degrees. The original response functions, which are shown as histograms, are seen to have several non-uniform variations between neighboring angular groups. By contrast the new response functions vary smoothly with emission angle. The agreement between the old and new response functions is generally very good, especially in the forward emission directions ($\phi \leq \pi/2$) shown in Fig. 4.1. Although the variation of the response functions in the backward directions is small, it should be noted that the new response functions are significantly lower (often by a factor of ten or more) compared to the original response functions. However, it should be noted that radiation emitted in such backward directions ($\phi > \pi/2$) almost always makes a very small contribution to the total skyshine dose.

In Fig. 4.2 the variation of the beam response functions with energy is illustrated for a fixed emission angle. Again, some unrealistic fluctuations in the response functions, particularly at high energies, are seen in the results obtained with the original response function coefficients. Also at lower energies, as a result of the coarse energy group structure and linear interpolation used, the original response functions are seen to vary only linearly with energy

and not to fall off as fast as one would expect. The results based on the new response function coefficients exhibit a smooth and much more realistic behavior.

4.2 Comparison with Monte Carlo Calculations

Response functions for point monodirectional source have been computed by Lynch et al. [Ly58] using Monte Carlo techniques. The results were reported in terms of tissue dose rather than air dose and are limited to source-detector distances from 5 to 100 ft (1.52 to 30.5 m) in air of density 0.00125 g/cm^3. Results are given for discrete energies between 0.6 and 12 MeV and at discrete emission angles between 1 and 180 degrees. Kitazume [Ki68] later confirmed these results using point kernel techniques and obtained good agreement at small emission angles and source-detector distances, and agreement within 20 percent over the entire range of calculations.

Comparison of the beam response functions calculated by Lynch et al. with those based on the beam coefficients presented here is somewhat complicated since Lynch's results are given in units of tissue dose while the present results are in air dose units. For photon energies between 0.1 MeV and 10 MeV, tissue dose exceeds air dose by about 10 percent. The two response functions are shown in Fig. 4.3 (each in its own dose units) as a function of source-detector distance for 2 MeV photons emitted at several angles. This comparison was chosen to illustrate angle and distance effects and is representative of similar comparisons at other source energies.

The agreement between these two sets of calculations is very close, with the Monte Carlo values being slightly higher as a result of their higher tissue dose response compared to the air dose response used for the beam functions. The new response functions presented here agree much more closely with Lynch's results at small angles than did the original beam response functions (a similar comparison for the RRA functions is given in [Fa87]). Part of this improved agreement is

attributable to the angular continuity in the new response functions. The RRA response functions, by contrast, used a discrete angular mesh with group boundaries often at the angles used by Lynch et al., thereby greatly complicating a direct comparison.

4.3 Comparison with Moments-Method Calculations

At the opposite extreme of the source emission restricted to a single direction is a completely uncollimated source emitting photons isotropically in all skyward directions. For this limiting 2π skyshine geometry, the detector response from skyshine at a given source-detector distance x is equal to half the response at the same source-detector distance resulting from photons originating from a bare point isotropic source and subsequently scattering in an infinite air atmosphere. It is thus possible to compare results of *MicroSkyshine* calculations, for this limiting case, with results of moments-method calculations for a point isotropic source in an infinite air medium.

MicroSkyshine calculations for such a comparison were performed in silo geometry with source and detector at the same elevation as the top of the silo with a 1 m radius. The source-detector distance x was varied from 25 to 2500 m, the photon energy E ranged from 0.1 to 10 MeV, and an air density of 1.25 mg/cm^3 was assumed. Infinite medium exposures due to scattered photons were deduced from air-kerma buildup factors computed using the method of moments by Chilton, Eisenhauer, and Simmons [Ch79]. If $R(E)$ is the exposure-rate response function (R m^2), $B(E,x)$ is the exposure buildup factor for photons of energy E at distance x in air of prescribed density, and $\mu(E)$ is the total interaction coefficient for photons of energy E in air of prescribed density, then the skyshine response, in units of R/photon, is given by

$$R = \frac{R(E)\ e^{-\mu(E)x}\ [B(E,x)\ -1]}{8\pi x^2}. \qquad (4.1)$$

The comparison of results from these two different methods of calculation is given in Fig. 4.4. The solid lines are results of *MicroSkyshine* calculations and the individual data points are results of the moments-method calculations. A similar comparison of these moments-method results with MicroSkyshine results based on the original RRA response functions is given by Faw and Shultis [Fa87]. The new response functions give results that are in far better agreement over a much greater source-detector distance than do the RRA response functions. For example, it was recommended that the RRA response functions be used only out to 1500m for energies greater than 1 MeV, and be restricted to even smaller distances for lower energies [Fa87]. With the new response functions, the *MicroSkyshine* method can now be accurately used for detector distances greater than 2500 m from the source for E greater than 1 MeV, and out to 1500 m for lower energies.

4.4 Skyshine Benchmark Calculations

In 1973 Working Group 6.6 was formed under the aegis of the Standards Committee of the American Nuclear Society to define standards for gamma skyshine radiation arising from LWR nuclear power plants. The resulting standard, currently under revision, is known as ANSI/ANS-6.6.1 [AN79]. In this standard, the Working Group provided four reference problems with results calculated by several computer programs. These reference problems are intentionally simplistic so as to facilitate the comparison of different calculational methods. The calculations presented in this standard are intended to provide some assurance that alternative methods used by a shielding analyst are in reasonable agreement with the reference calculational methods.

4.4.1 ANSI/ANS-6.6.1 Reference Problems

The first Reference Problem I.1 is for a bare, point, isotropic

source of ^{16}N gamma photons with energies of 6.2 MeV. The source, which has a strength of 1 photon per second, is positioned 60 ft (18.3 m) in air above a horizontal air-ground interface. Detectors are placed at distances from 200 ft (61 m) to 5000 ft (1,500 m) from the normal through the source to the ground-interface and at a height of 3 ft (0.91 m) above grade. The problem geometry is shown in Fig. 4.5. The detector response is to be calculated for the total dose rate (in units of rads(air)/yr) as well as for the skyshine component alone.

The second Reference Problem places the source of Problem I.1 on the vertical axis of a rectangular roofless building having 4 ft (1.22 m) thick concrete walls on all four sides. The source is 60 ft (18.3 m) above grade and the building sides at 62 ft (18.9 m) high. The detectors are located as in Problem I.1. The inside dimensions of the enclosure are 100 ft (30.5 m) by 150 ft (45.7 m) and the building is oriented so that the long walls are perpendicular to the line of detectors. The geometry for this problem is shown in Fig. 4.6. Again the detector response is to be calculated for the total dose rate (in rads (air) per year) and for only the skyshine component.

In all the reference calculations the air density is to be taken as 1.22 mg/cm^3 with a number density of 1.07×10^{19} $atoms/cm^3$ of oxygen and 4.02×10^{19} $atoms/cm^3$ of nitrogen. The density of concrete is to be taken as 2.34 g/cm^3 with the following composition:

Concrete Composition

Element	$Atoms/cm^3$	Element	$Atoms/cm^3$	Element	$Atoms/cm^3$
H	7.86×10^{21}	Mg	1.40×10^{20}	K	6.90×10^{20}
O	4.38×10^{22}	Al	2.39×10^{21}	Ca	2.92×10^{21}
Na	1.05×10^{21}	Si	1.58×10^{22}	Fe	3.10×10^{20}

If the ground can be treated by the analysis code, the soil density is to be taken as 1.7 g/cm^3 with the following composition:

Ground Composition

Element	Atoms/cm^3	Element	Atoms/cm^3
H	9.77×10^{21}	Al	4.88×10^{21}
O	3.48×10^{22}	Si	1.16×10^{22}

4.4.2 Methods Used for Reference Calculations

The ANSI/ANS-6.6.1 Reference Problems were solved by several codes using a variety of radiation transport techniques. Specifically, the following codes were used:

(a) DOT II [My73]: This a two-dimensional, discrete ordinates, general-purpose transport code that uses an energy multigroup approximation and allows for anisotropic scattering.

(b) OGRE [Pe65]: This is a Monte Carlo code specifically designed for gamma transport problems.

(c) COHORT II [So75]: This is a specialized Monte Carlo code designed for shielding calculations.

(d) QADMOD [Pr74]: This is a three-dimensional point-kernel code based on the single scatter approximation.

(e) SKREEN [Ro73]: This is a point-kernel shielding code.

(f) G^3 [Ma73]: This a three-dimensional, single-scatter (point kernel) code especially suitable for photon skyshine calculations.

(g) SKYSHINE [Pr76]: This code numerically integrates empirically derived beam response functions (based on Monte Carlo results) to find skyshine dose rates.

The results obtained with these codes were based on a variety of different assumptions and simplifications to the reference problems. For example, several calculations ignored the presence of the ground by simply replacing it by an infinite air medium. Moreover, different energy-group structures and different cross-section libraries were used. Yet despite these differences and approximations, the reported results

are all in reasonable agreement and serve as excellent standards against which to compare other calculational schemes.

4.4.3 Comparison of Results for ANSI Problem I.1

To adapt *MicroSkyshine* to ANSI/ANS-6.6.1 Reference Problem I.1 (see Fig. 4.7), the point N-16 source was placed on the axis of an open silo of 1 m inner radius and with walls 60 ft (18.3 m) high. The source and detector were placed 0.000001 m below this elevation so as to eliminate any direct (unscattered) component. The source-to-detector distance in this *MicroSkyshine* calculation was then interpreted as the slant distance x between the source and detector in the reference problem. The horizontal range r in the reference problem is related to this slant distance by

$$r = \left[x^2 - (\Delta z)^2 \right]^{1/2} \qquad (4.2)$$

where Δz is the difference in elevation between source and detector in the reference problem (17.4 m).

In Fig. 4.7 the *MicroSkyshine* results using the improved response functions are plotted as a solid line and those obtained with the original RRA response functions are shown by the dashed line. The results of the seven other calculations reported in the ANSI standard are shown as discrete points. (To maintain consistency between this comparison and other results in this report, the scales of the figure have been changed from those in ANSI Standard 6.6.1 so that range is in meters and dose in rad/yr.) It is seen from Fig. 4.7 that both *MicroSkyshine* results are in excellent agreement with the earlier calculations. However, the asymptotic behavior of the results based on the new response functions at large distances from the source are in much better agreement with the benchmark results than values based on the original RRA response functions.

4.4.4 Comparison of Results for ANSI Problem I.2

ANSI/ANS-6.6.1 Reference Problem I.2 collimates a point isotropic source (E = 6.12 MeV) by an open rectangular building. The geometry is shown in Fig. 4.8. To apply *MicroSkyshine* to this problem, it is first necessary to modify slightly the treatment of the infinite wall geometry so that rays from the source would be limited not only by the front wall (i.e., wall closest to the detectors) but also by the side and rear walls.

The results of this calculation using the new response functions (solid line) and the original RRA response functions (dashed line) are shown in Fig. 4.8 along with the four results reported by the ANSI 6.6.1 Standard. In addition, SKYSHINE II results [La79] also shown and it is not surprising that they agree very closely with the dashed-line *MicroSkyshine* results since both are based on the same PRIGAM response functions (although they differ in how the functions are used to evaluate the skyshine). It is see from Fig. 4.8 that the new response functions produce asymptotic results that are in better agreement with the reference benchmark calculations than those obtained with the original RRA response functions.

4.5 Comparison With Benchmark Skyshine Experiments

4.5.1 Description of Experiments

There are few experimental skyshine measurements which can serve as benchmarks for the skyshine problem. Most measurements have been taken relatively near the source ($\lesssim$ 1 mean free path in air) or involve geometric configurations which are too difficult to model accurately. To alleviate this deficiency, several years ago a major experimental program, designed for ease of simulation, was performed to measure the skyshine radiation over a source-to-detector baseline from 30 to 700 m [Na81]. Data from this experiment serve as standards against which

calculational models can be tested.

The benchmark experiment described here was performed at the Kansas State University Nuclear Engineering Shielding Facility as part of a project managed by Radiation Research Associates under support and guidance of the Japanese Nuclear Safety Research Association Study Committee on Air-Scattered Gamma Rays in Nuclear Facilities. Compact cobalt-60 sources with activities up to 140 GBq (5200 curies) were position on the axis of an annular concrete silo with walls sufficiently thick to preclude significant radial penetration of radiation. Two basic experimental geometries were used (see Fig. 4.9). In the "unshielded" geometry, wedge-shaped collimator concrete blocks were placed around the top edge of the silo wall so as to define an open conical aperture with a full-angle of 150.5 degrees and with the source at the apex. In the "shielded" geometry, concrete shielding slabs of two thicknesses (21 or 43 cm) and of density 2.13 g/cm^3 were placed atop the silo.

With the above source geometries, two types of skyshine measurements were made. With a well-collimated and shielded NaI detector, energy spectral measurements of the skyshine 2.2 m above grade were obtained radially outwards in 100-m increments out to 700 m from the source. In a second set of measurements, which are of more interest to the present study, a high-pressure ionization chamber was used to measure directly the 4π-skyshine-exposure rate 1 m above grade at distances from 30 m out to 700 m from the silo axis.

4.5.2 Experimental Results

Several corrections were made to the raw experimental data. Although the energy sensitivity of the high pressure ionization chamber was relatively flat for high gamma-ray energies (> 300 keV), it varied significantly for lower energies (where the measured skyshine spectra was found to peak). Using the measured skyshine energy spectra, a correction factor to account for the non-uniform energy response of the

detector was calculated. Typically, less than a 10% correction was needed to obtain the true skyshine exposure rate.

It was also possible to infer exposure rates from the NaI spectral measurements. Using measured energy response functions based on NBS calibration sources, the NaI spectra were unfolded. The unfolded spectra were then integrated over energy to give exposure rates and then further corrected for the NaI collimation. These secondary or derived skyshine exposure rates were found to be in excellent agreement with those obtained with the high-pressure ionization chamber.

4.5.3 Comparison of Calculated and Measured Results

To facilitate the comparison, the results of the MicroSkyshine calculations have been expressed in the same format as those of the experimental data. The independent variable is the areal density separating source and detector, *i.e.*, the product of the air density and the source detector distance. Use of the areal density minimizes effects of day-to day variations in air density experienced during the course of the exper iments. The dependent variable is the exposure per photon multiplied by the square of the source-detector distance and divided by the solid angle of collimation, namely 4.683 sr. In this form, the strong effect of source-detector distance on detector response, through the inverse-square law, is suppressed.

The skyshine exposure rates for the three experiment configurations (bare, 21 cm shield, and 43 cm shield) are shown in Fig. 4.10 along with the predictions obtained with *MicroSkyshine* and the new response functions. The agreement between calculated and measured results is excellent. In particular, the asymptotic slopes between the experimental and calculated values are seen to be very close. Similar calculations using the original RRA response functions (see [Fa87]) yielded results that did not fall off as rapidly at large source-to-detector distances. Moreover, the original RRA response functions

predicted skyshine doses that were 30-80% higher for areal densities greater than 20 g/cm^2 (distances greater than about 160 m).

4.5.4 Comparison with Hybrid ANISN/SKYSHINE-II Calculations

Keck and Herchenroder [KeS2] performed calculations for the conditions of the KSU benchmark experiments, with concrete overhead shielding, using a hybrid technique. They first used the ANISN one-dimensional discrete-ordinates transport code to estimate the energy and angular distributions of the gamma rays emerging from the top surface of the overhead concrete shield. Treating the upper shield surface as a secondary source, they then used the SKYSHINE-II code [La79] to calculate skyshine dose rates. Their results, which agree very well with experimental results, are illustrated in Fig. 4.11 along with *MicroSkyshine* results for the same conditions. The *MicroSkyshine* results, based on the new response functions, are seen to be in good agreement and agree much better at large distances from the source than do results based on the original RRA response functions [see FaS7 for results].

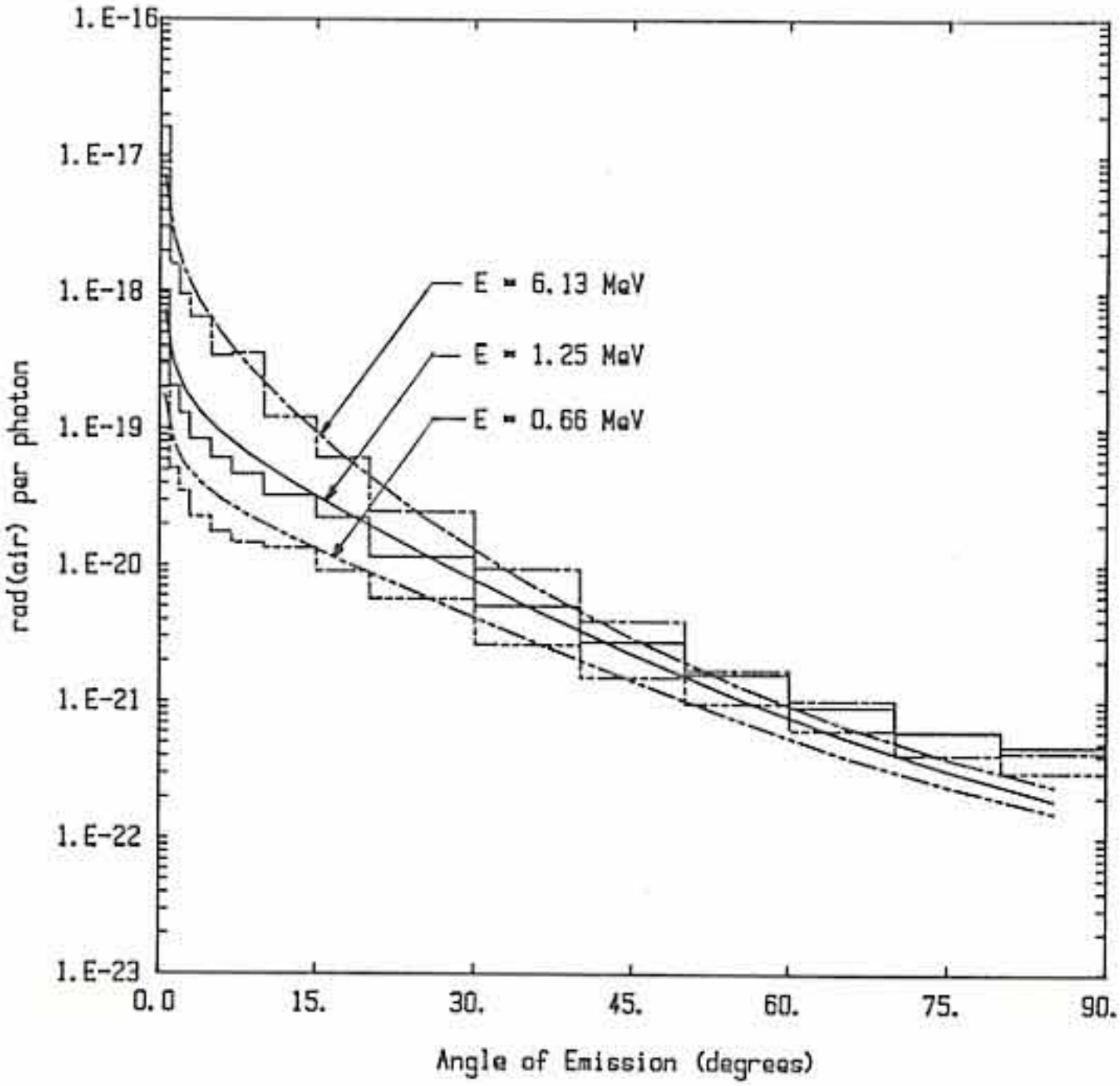

Fig. 4.1 Variation of the PRIGAM atmospheric scattering response function $R(E,\phi,x)$ with angle of photon emission ϕ at fixed source-detector distance x = 500 m and at selected photon energies. Histogram: original RRA response functions based on Monte Carlo calculations [La79]. Lines: new response functions based on point-kernel calculations reported here.

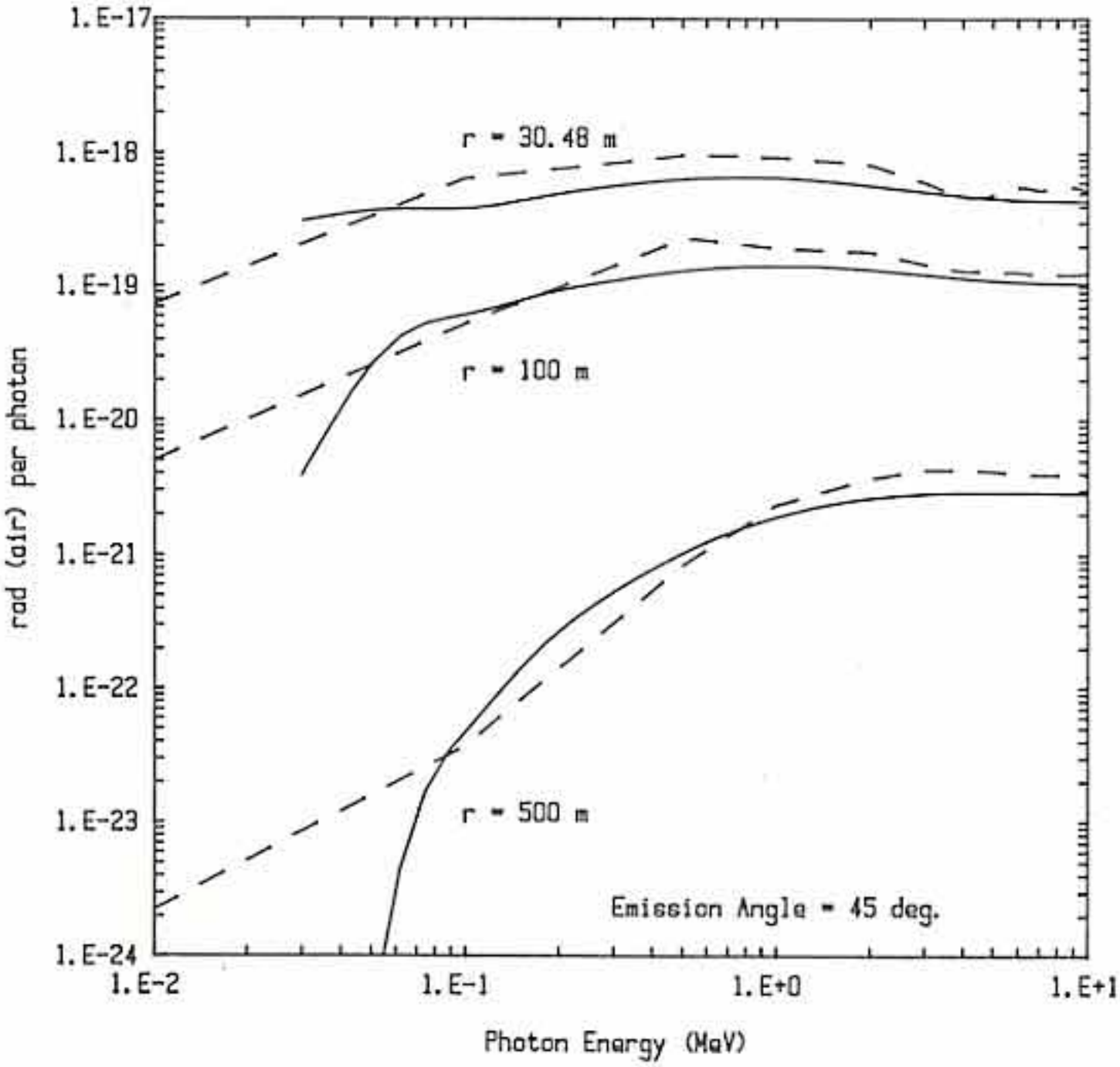

Fig. 4.2 Variation of the PRIGAM atmospheric scattering response function $R(E,\phi,x)$ with photon energy E at fixed angle of emission ϕ and at selected source-detector distances. Broken lines: original RRA response functions based on Monte Carlo calculations [La79]. Solid lines: new response functions based on point-kernel calculations reported here.

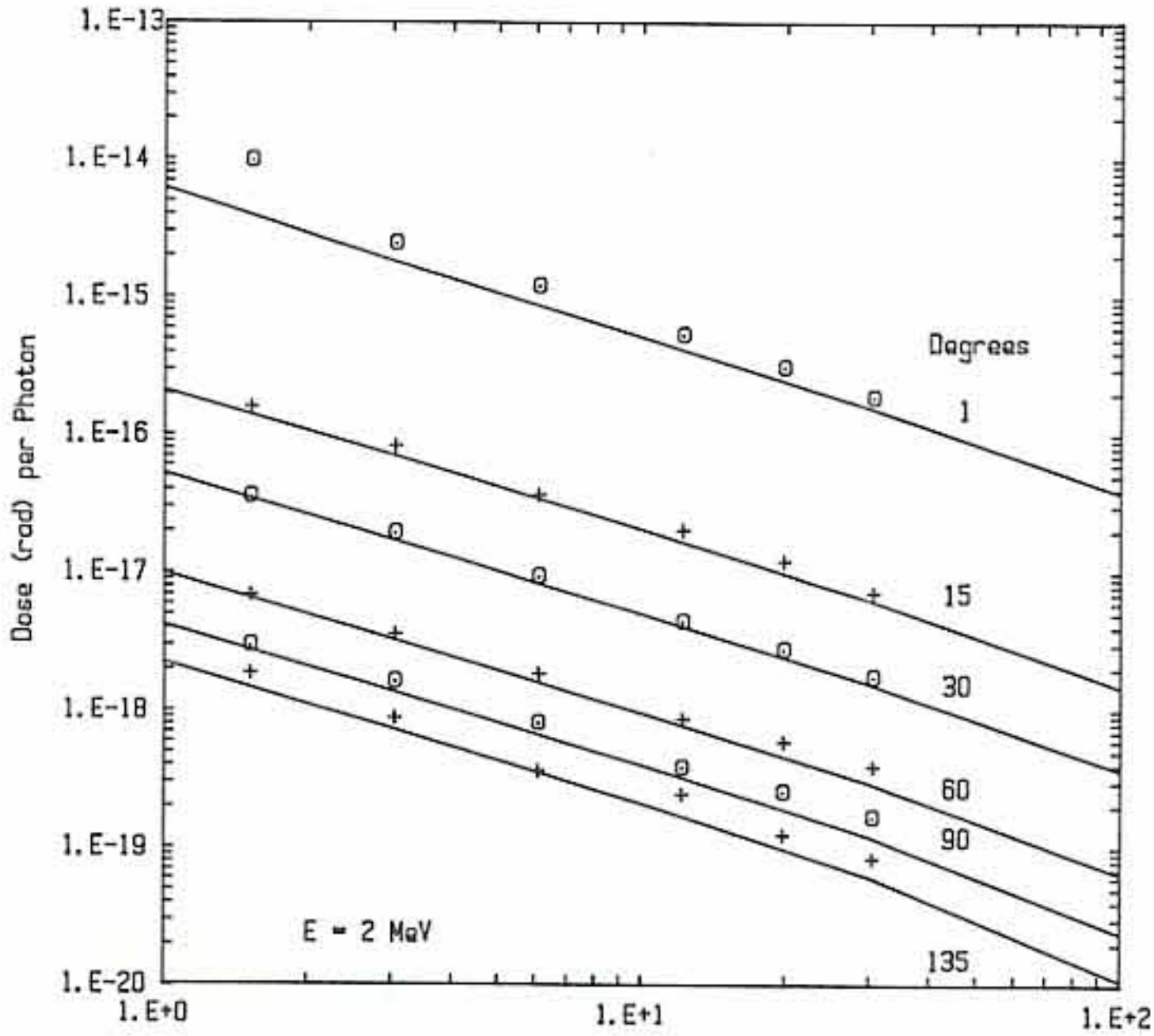

Fig. 4.3 Comparison of new PRIGAM atmospheric scattering response functions (solid lines) with response functions calculated by Lynch, et al. [Ly58] for 2-MeV photons at selected angles of emission.

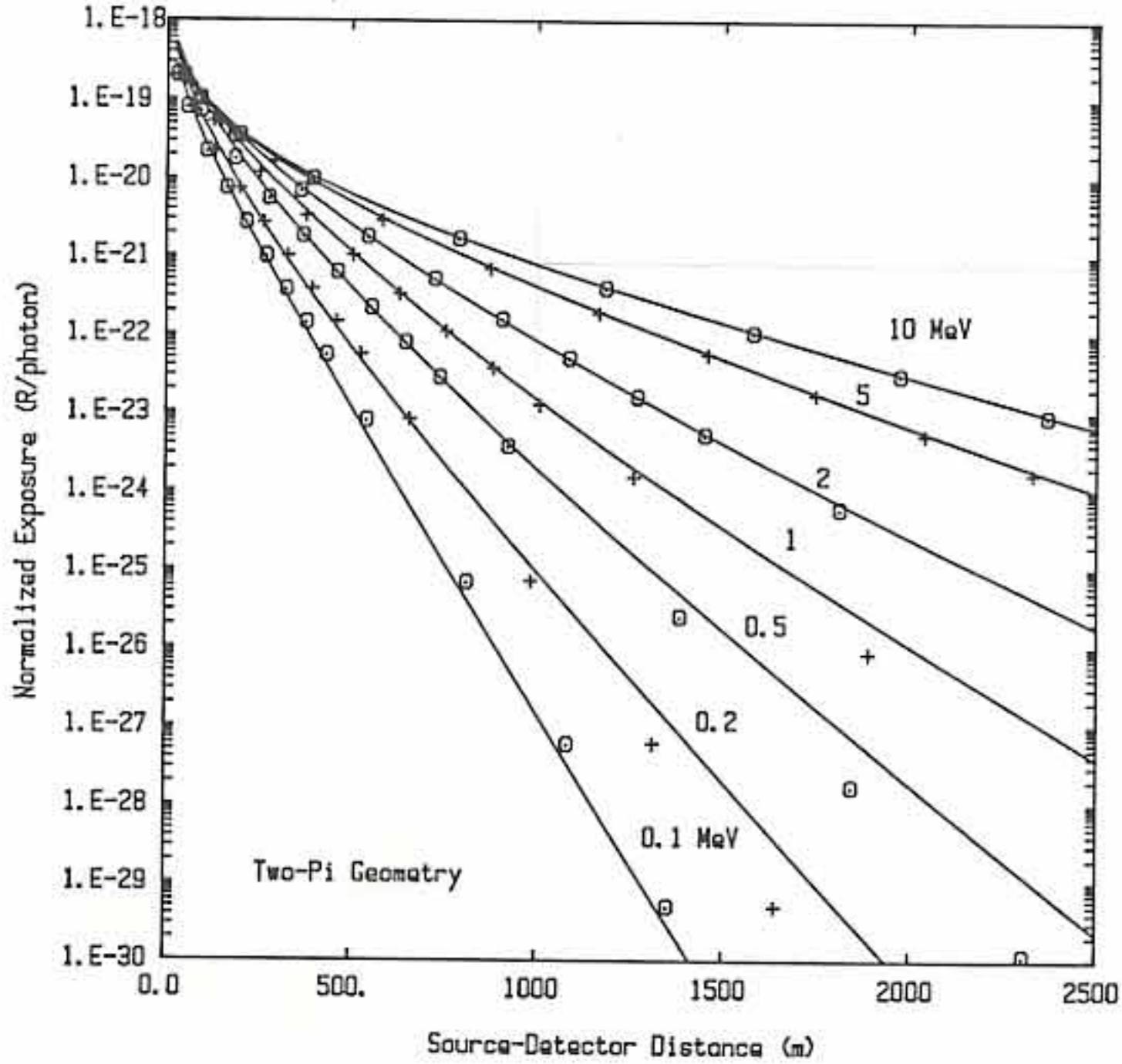

Fig. 4.4 Comparison of MicroSkyshine results (solid lines) with moments-method results (data points) for the scattered-radiation dose arising from a point source emitting photons only in the 2π-steradian upward hemisphere of directions in an infinite atmosphere.

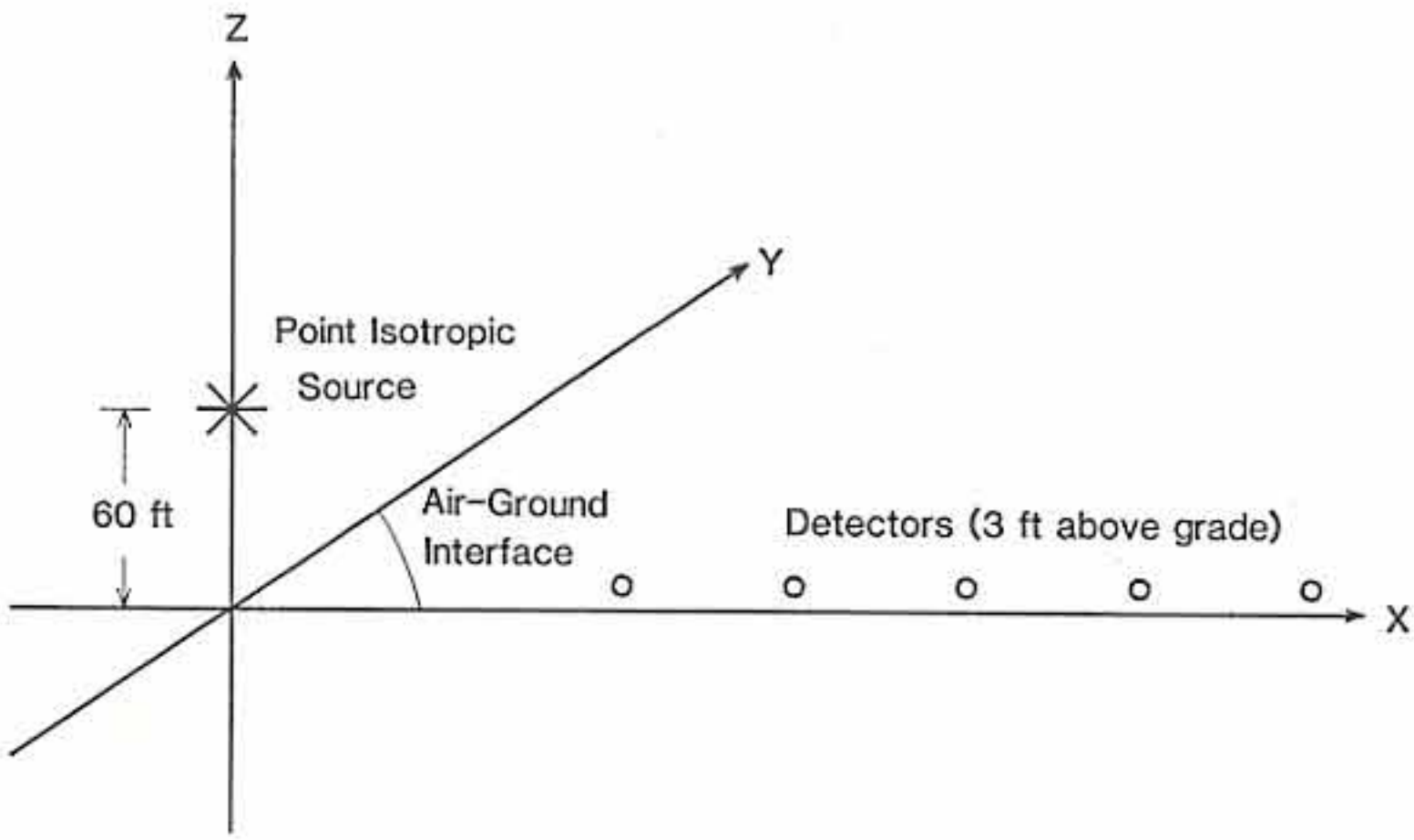

Fig. 4.5. Geometry for ANSI/ANS-6.6.1 Reference Problem I.1.

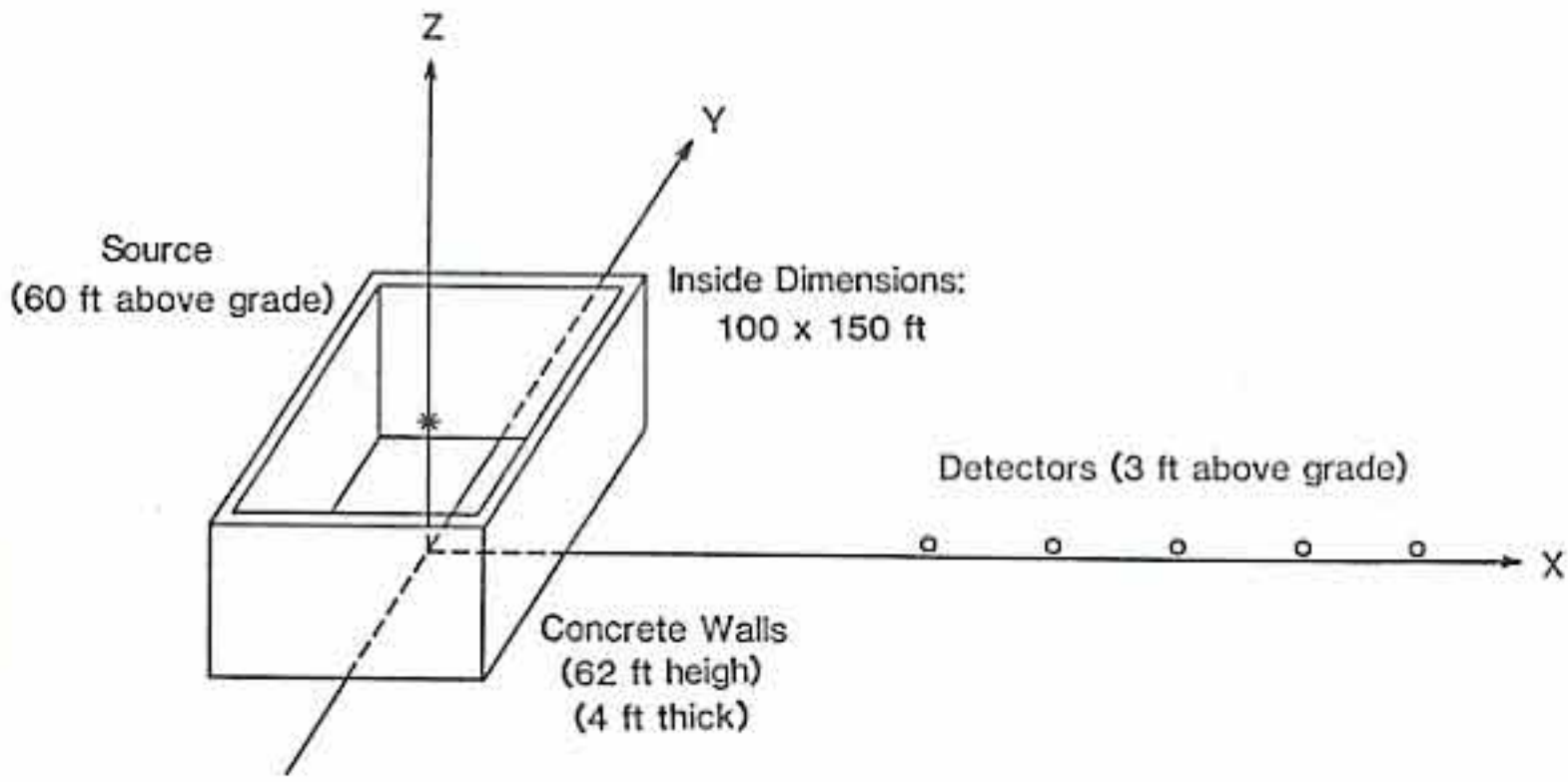

Fig. 4.6. Geometry for ANSI/ANS-6.6.1 Reference Problem I.2.

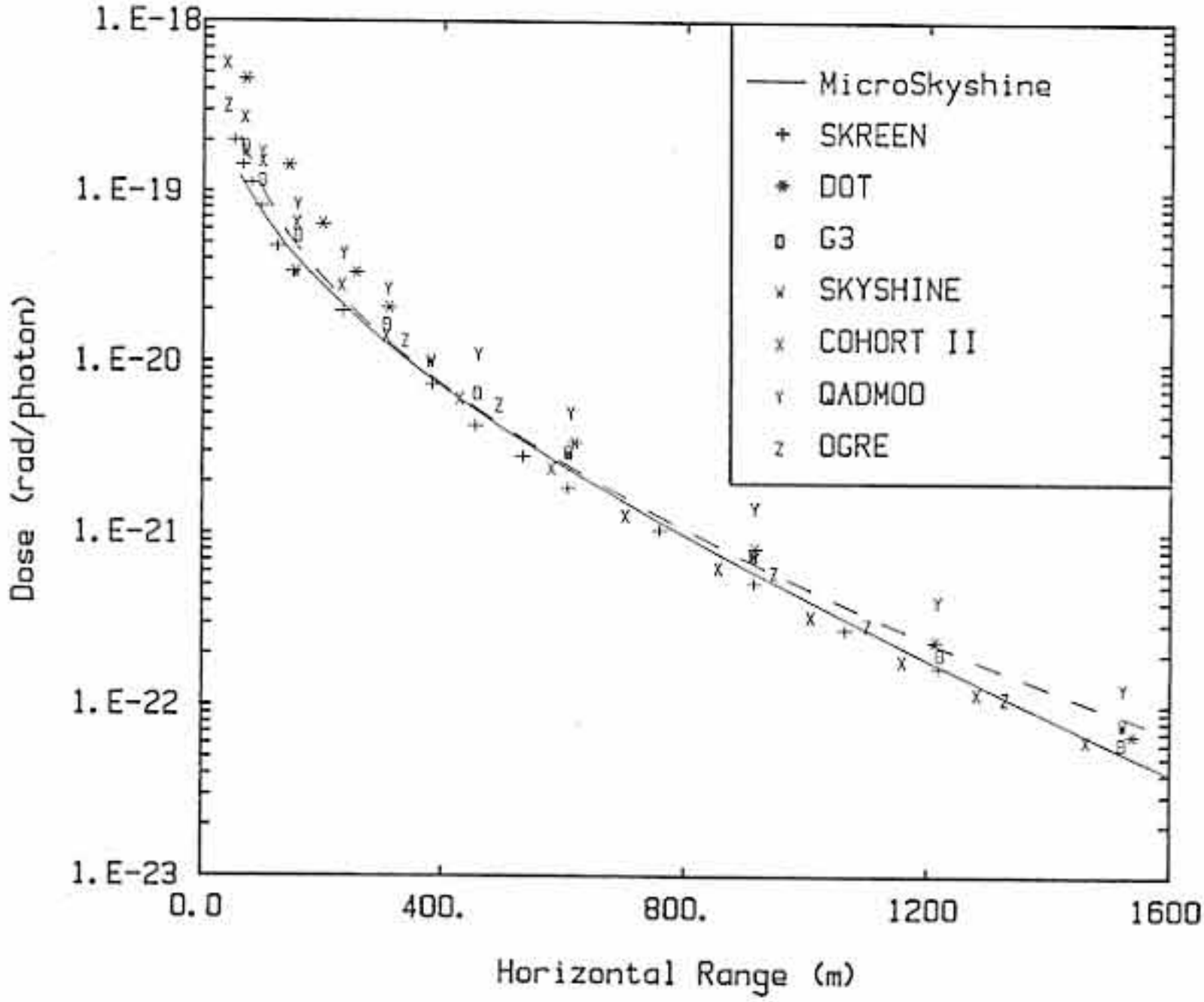

Fig. 4.7 Comparison of MicroSkyshine calculations with benchmark calculations for ANSI/ANS-6.6.1 Reference Problem I.1. Broken lines: *MicroSkyshine* calculations based on original RRA response functions [La79]. Solid lines: *MicroSkyshine* calculations based on new point-kernel response functions reported here.

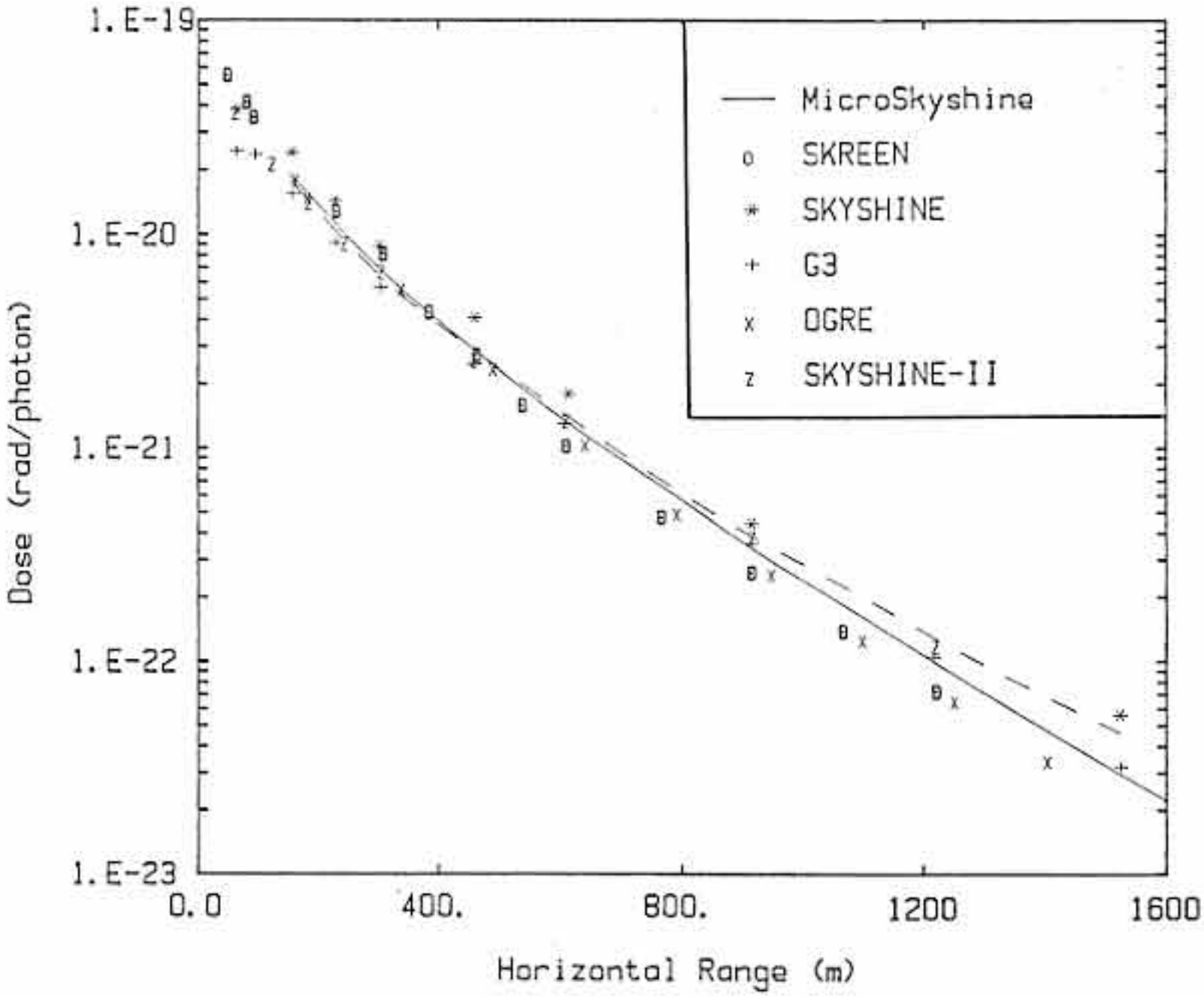

Fig. 4.8 Comparison of MicroSkyshine calculations with benchmark calculations for ANSI/ANS-6.6.1 Reference Problem I.2. Broken lines: *MicroSkyshine* calculations based on original RRA response functions [La79]. Solid lines: *MicroSkyshine* calculations based on new point-kernel response functions reported here.

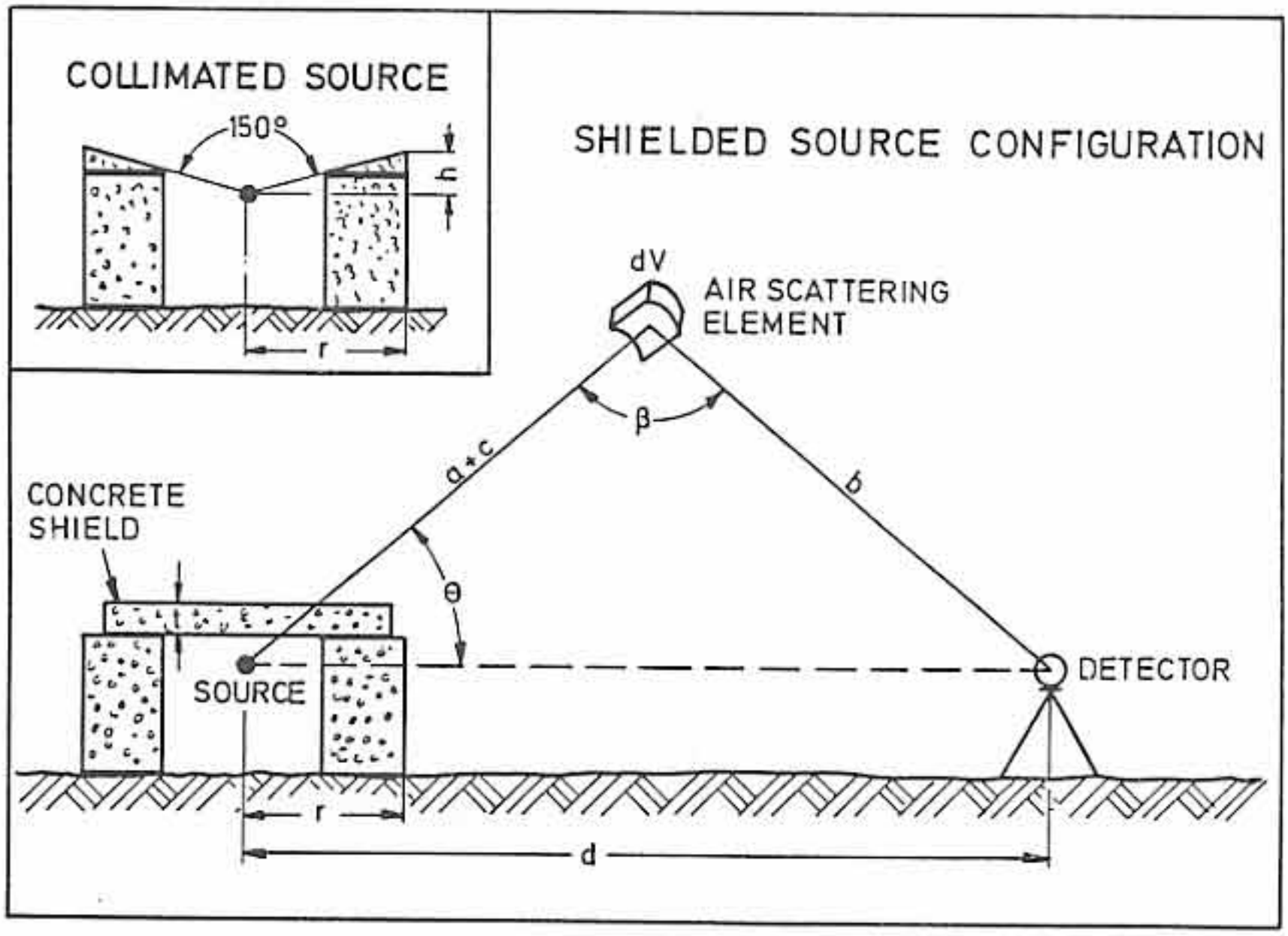

Fig. 4.9 Geometry for benchmark skyshine experiments. Source is in a concrete annular cylinder (2.5-m i.d., 4.35-m o.d., 2.29-m height) and either shielded from above by a concrete slab (21.0 or 42.8 cm thick) or collimated into a 150.5-degree vertical cone (inset). Distances a and b refer to the air path distances between the source and scattering element and between the scattering element and the detector respectively. Ray distance through concrete is denoted by c.

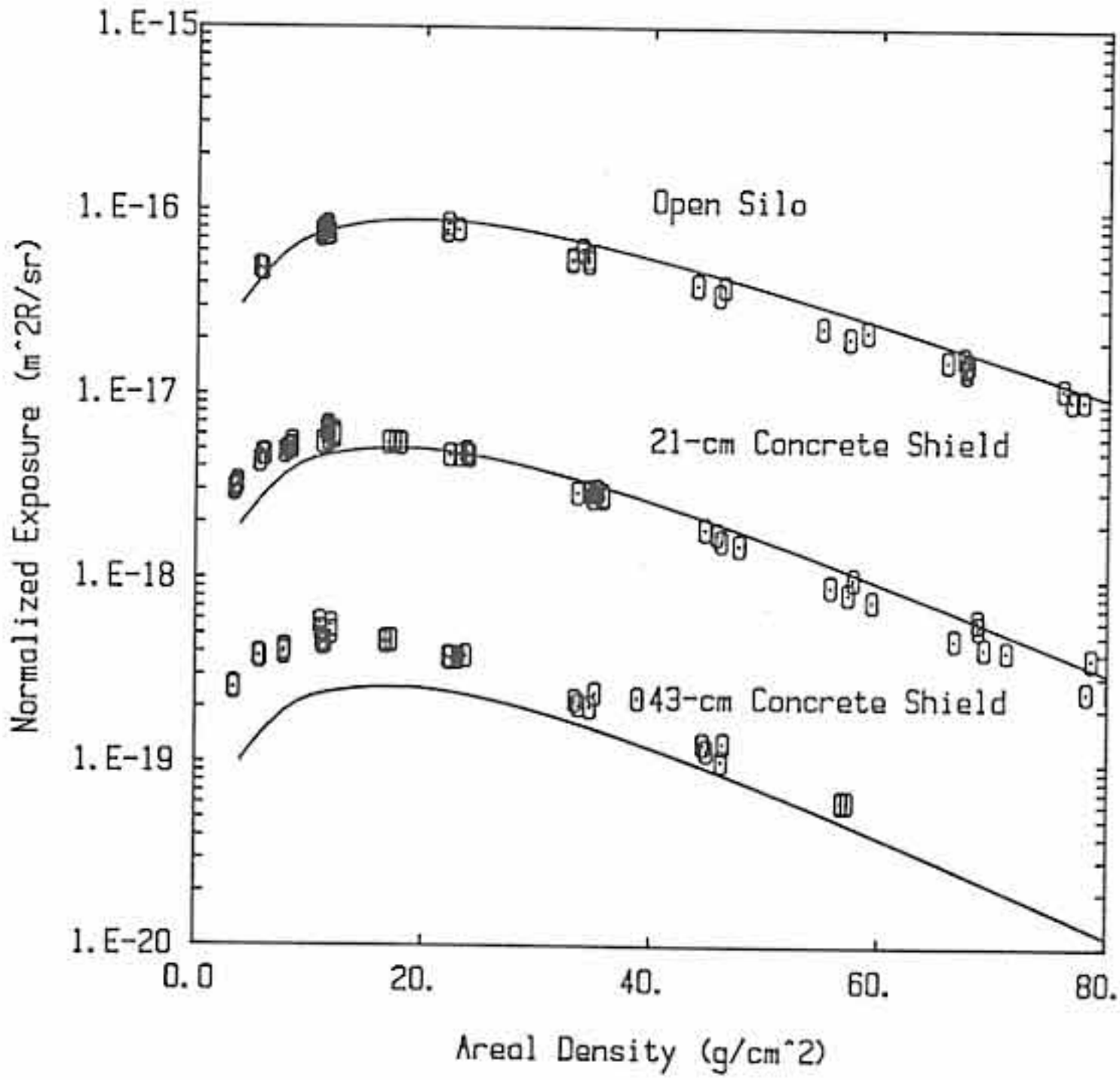

Fig. 4.10 Comparison of *MicroSkyshine* results (solid lines) with experimental data for the conditions of the KSU benchmark skyshine experiments. A ^{60}Co source is within a cylindrical silo with a 150.5-degree full-angle of collimation. Three cases are shown: (1) no overhead shielding, (2) 21 cm of overhead concrete shielding, and (3) 42.8 cm of overhead concrete shielding of density 2.32.g/cm^3.

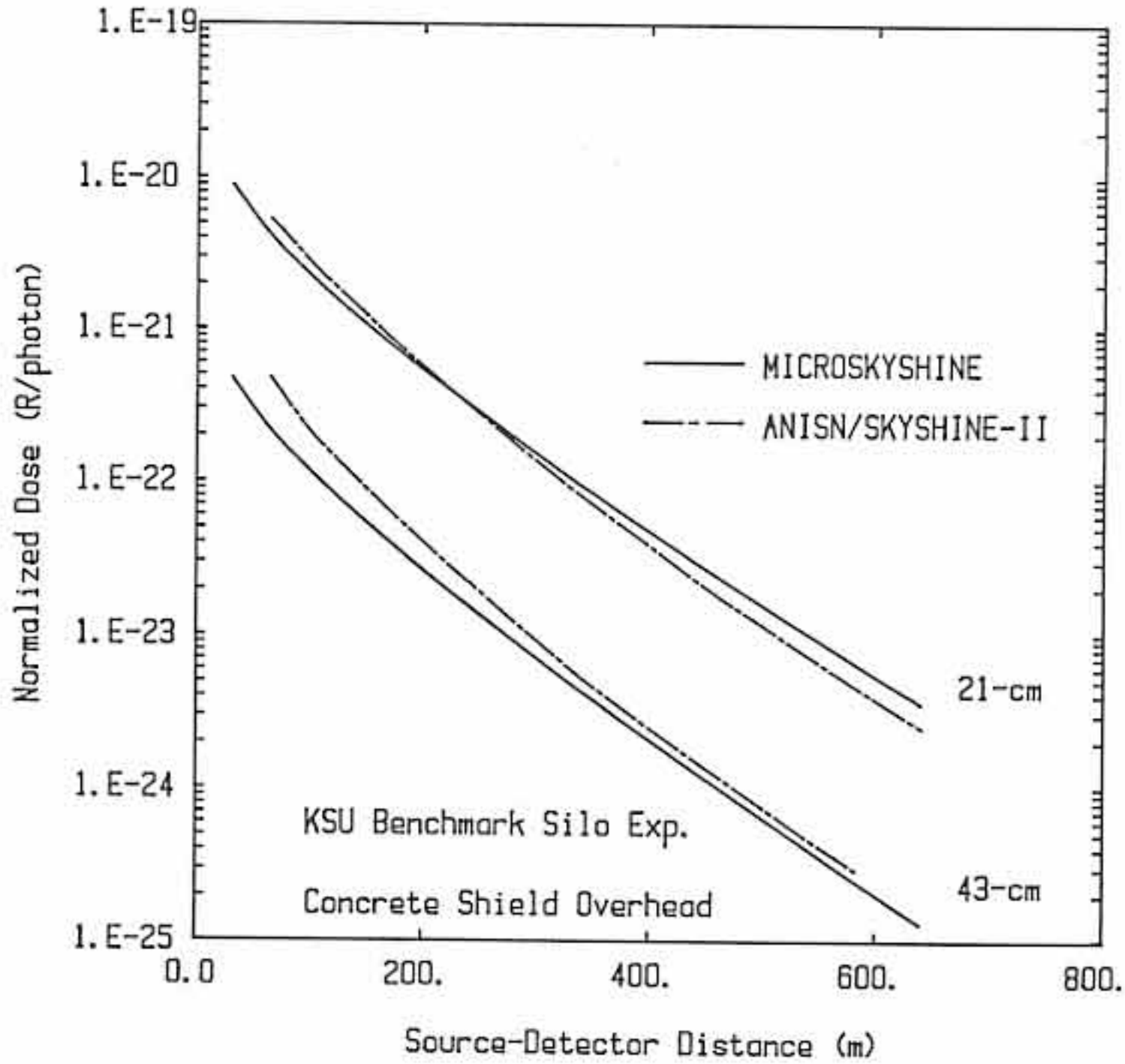

Fig. 4.11 Comparison of *MicroSkyshine* results (solid lines) with hybrid ANISN/SKYSHINE-II results [Ke82] (broken lines) for the conditions of the KSU benchmark skyshine experiments with overhead shielding.

5. Bibliography

An79 ANSI/ANS-6.6.1-1979, *American National Standard for Calculation and Measurement of of Direct and Scattered Gamma Radiation from LWR Nuclear Power Plants*, American Nuclear Society, LaGrange Park, Illinois, 1979.

Ch79 Chilton, A. B., "Tschebycheff-Fitted Berger Coefficients for Eisenhauer-Simmons Gamma-Ray Buildup Factors in Ordinary Concrete," **Nucl. Sci. & Engg.**, 69, 436-438 (1979).

Ch84 Chilton, A. B., J. K. Shultis, and R. E. Faw, *Principles of Radiation Shielding*, Prentice-Hall, 1984.

Fa87 Faw, R. E., and J. K. Shultis, *The MicroSkyshine Method for Gamma-Ray Skyshine Analysis*, Report-188, Engineering Experiment Station, Kansas State University, Manhattan, KS 1987.

Gr87 *MicroSkyshine Users' Manual* (Draft), Grove Engineering, Inc., 15215 Shady Grove Rd., Rockville, MD 20950, 1987.

HS33 Harima, Y., "An Approximation of Gamma-Ray Buildup Factors by Modified Geometric Progression," **Nucl. Sci & Engg., 83**, 299-309 (1983).

Ha86 Harima, Y., Y. Sakamoto, S. Tanaka, and M. Kawai, "Validity of the Geometric-Progression Formula in Approximating Gamma-Ray Buildup Factors, **Nucl. Sci. & Engg., 94**, 24-35 (1986).

Hu82 Hubbell, J. H., **Int. J. Appl. Radiat. Isot., 33**, 1269-1290 (1982).

Ke82 Keck, B., and P. Herchenroder, Nachrechnen eines Gamma-Skyshine-Benchmarkexperiments," **Atomwirtschaft**, May, 1982.

Ki68 Kitazume, Mitsuyuki, "A Simplified Calculation for Air-Scattered Gamma Rays," **J. Nucl. Sci. & Tech**, 5, 464-471 (1968).

Ko68 Kowalik, J., and M. R. Osborne, *Methods for Unconstrained Optimization Problems*, Elsevier, New York, 1968, p. 24.

La79 Lampley, C. M., The Skyshine-II Procedure: *Calculation of the Effects of Structure Design on Neutron, Primary Gamma-Ray, and Secondary Gamma-Ray Dose Rates in Air*, Report RRA-T7901 (NUREG/CR-0781), Radiation Research Associates, Fort Worth, Texas, 1979.

Ly58 Lynch, R. E., J. W. Benoit, W. P. Johnson, and C. D. Zerby, *A Monte Carlo Calculation of Air-Scattered Gamma Rays*, Report ORNL 2292, Oak Ridge National Laboratory, Oak Ridge, Tennessee, 1958.

Ma73 Malefant, Richard E., G^3: *A General Purpose Gamma-Ray Scattering Program*, Report LA-5176, Los Alamos Scientific Laboratory, Los Alamos, New Mexico, 1973.

My73 Mynatt, F. R., et al., *The DOT II Two-Dimensional Discrete-Ordinates Transport Code*, Report ORNL-TM-4280, Oak Ridge National Laboratory, Oak Ridge, Tennessee, 1973.

Na81 Nason, R. R., J. K. Shultis, R. E. Faw, and C. E. Clifford, "A Benchmark Gamma-Ray Skyshine Experiment," **Nucl. Sci. & Engg.**, 79, 404-416 (1981).

Pe65 Penny, S. K., D. K. Trubey, and M. B. Emmett, *OGRE, A Monte Carlo System for Gamma Ray Transport Studies, Including an Example, (OGRE-P1) for Transmission through Laminated Slabs*, Report ORNL-3905, Oak Ridge National Laboratory, Oak Ridge, Tennessee, 1965.

Pr76 Price, J. H., D. G. Collins, and M. B. Wells, *Utilization Instructions for SKYSHINE*, Report RRA-N7608, Radiation Research Associates, Fort Worth, Texas, 1976.

Ro73 Rogers, D.R., *BWR Turbine Equipment ^{16}N Radiation Shielding Studies*, Report NEDO-20206, General Electric Company, San Jose, California, 1976.

Rs86 *Documentation for CCC-493B/QAD-CGCP Code Package*, Report CCC-493, Radiation Shielding Information Center, Oak Ridge National Laboratory, Oak Ridge, Tennessee, 1986.

So75 Soffer, L., and L. C. Clemons, Jr., *COHORT-II: A Monte Carlo General Purpose Shielding Computer Code*, Report NASA-TN-D-6170, Lewis Research Center, Cleveland, Ohio.

St67 Storm, E., and H. I. Israel, *Photon Cross Sections from 0.001 to 100 MeV for Elements 1 through 100*, Report LA-3753, Los Alamos Scientific Laboratory, Los Alamos, New Mexico, 1967.

APPENDIX A

Coefficients for the Line-Beam Gamma-Ray Response Functions

Source Energy: 9.5 MeV

Angle (deg)	Coefficient a	Coefficient b	Coefficient c	Av. MAD (%)	Max. Dev. (%)
0.5	-8.91568	-0.99301	0.00248	0.3	0.4
1.5	-10.14431	-0.97954	0.00243	0.8	-0.8
2.5	-10.78282	-0.96765	0.00243	1.1	-1.3
4.0	-11.43880	-0.95306	0.00245	1.6	-1.8
6.0	-12.08827	-0.93680	0.00252	1.9	-2.3
8.5	-12.73211	-0.91973	0.00263	2.2	2.7
12.5	-13.56202	-0.89569	0.00288	2.4	3.3
17.5	-14.38304	-0.86783	0.00329	2.3	3.8
25.0	-15.31173	-0.82844	0.00404	2.1	4.5
35.0	-16.22773	-0.77307	0.00518	2.1	5.2
45.0	-16.93617	-0.71375	0.00636	2.4	6.3
55.0	-17.55317	-0.64425	0.00752	3.2	8.2
65.0	-18.13527	-0.56366	0.00859	4.9	11.2
75.0	-18.67047	-0.48302	0.00948	8.6	14.6
85.0	-18.93738	-0.46223	0.01000	10.3	15.6
95.0	-18.90293	-0.51104	0.01016	8.8	13.8
110.0	-18.76997	-0.59498	0.01017	6.6	10.7
130.0	-18.69541	-0.66378	0.01013	5.8	8.8
150.0	-18.68741	-0.69790	0.01011	5.8	8.1
170.0	-18.68751	-0.71336	0.01010	5.9	7.9

Source Energy: 8.5 MeV

Angle (deg)	Coefficient a	Coefficient b	Coefficient c	Av. MAD (%)	Max. Dev. (%)
0.5	-8.83156	-0.99313	0.00258	0.3	0.3
1.5	-10.06015	-0.97856	0.00253	0.8	-0.9
2.5	-10.69426	-0.96639	0.00253	1.2	-1.4
4.0	-11.34385	-0.95118	0.00255	1.6	-1.9
6.0	-11.98481	-0.93399	0.00261	2.0	-2.4
8.5	-12.62155	-0.91565	0.00273	2.4	2.9
12.5	-13.43509	-0.89185	0.00297	2.6	3.5
17.5	-14.25599	-0.86217	0.00338	2.6	4.1
25.0	-15.19481	-0.82114	0.00411	2.6	4.9
35.0	-16.13103	-0.76409	0.00523	2.5	5.9
45.0	-16.85502	-0.70466	0.00639	2.8	7.0
55.0	-17.47239	-0.63802	0.00753	3.6	8.9
65.0	-18.03689	-0.56408	0.00858	5.6	11.5
75.0	-18.54096	-0.49259	0.00947	8.9	14.5
85.0	-18.80175	-0.47461	0.00999	10.3	15.3
95.0	-18.77677	-0.52247	0.01016	8.7	13.5
110.0	-18.64283	-0.60839	0.01017	6.3	10.3
130.0	-18.56277	-0.67994	0.01013	5.4	8.2
150.0	-18.55371	-0.71538	0.01010	5.4	7.5
170.0	-18.55547	-0.73088	0.01009	5.5	7.3

Source Energy: 7.5 MeV

Angle (deg)	Coefficient a	Coefficient b	Coefficient c	Av. MAD (%)	Max. Dev. (%)
0.5	-8.73586	-0.99324	0.00271	0.3	0.3
1.5	-9.96185	-0.97802	0.00266	0.8	0.9
2.5	-10.59345	-0.96502	0.00265	1.3	-1.4
4.0	-11.23784	-0.94879	0.00267	1.7	-2.0
6.0	-11.86703	-0.93148	0.00273	2.2	-2.5
8.5	-12.48963	-0.91315	0.00284	2.5	3.0
12.5	-13.29309	-0.88770	0.00308	2.8	3.7
17.5	-14.10896	-0.85694	0.00348	3.0	4.4
25.0	-15.05540	-0.81451	0.00420	3.1	5.4
35.0	-16.01343	-0.75538	0.00530	3.2	6.5
45.0	-16.74823	-0.69705	0.00643	3.5	7.7
55.0	-17.36967	-0.63302	0.00755	4.5	9.5
65.0	-17.91529	-0.56660	0.00858	6.3	11.8
75.0	-18.39054	-0.50408	0.00945	9.1	14.3
85.0	-18.64464	-0.48929	0.00998	10.2	15.0
95.0	-18.63231	-0.53571	0.01016	8.6	13.2
110.0	-18.49817	-0.62380	0.01017	6.0	9.9
130.0	-18.41410	-0.69875	0.01012	4.9	7.6
150.0	-18.40158	-0.73612	0.01009	4.9	6.7
170.0	-18.40473	-0.75195	0.01008	5.0	6.5

Source Energy: 6.5 MeV

Angle (deg)	Coefficient a	Coefficient b	Coefficient c	Av. MAD (%)	Max. Dev. (%)
0.5	-8.63775	-0.99052	0.00289	0.4	-0.5
1.5	-9.87913	-0.96994	0.00284	1.2	1.6
2.5	-10.51728	-0.95374	0.00283	1.7	2.3
4.0	-11.16730	-0.93379	0.00285	2.3	3.1
6.0	-11.79500	-0.91359	0.00292	2.8	3.7
8.5	-12.41234	-0.89270	0.00303	3.2	4.2
12.5	-13.20231	-0.86576	0.00326	3.5	4.6
17.5	-14.00646	-0.83481	0.00365	3.6	5.3
25.0	-14.96438	-0.78976	0.00435	3.8	6.3
35.0	-15.92977	-0.73124	0.00542	4.1	7.8
45.0	-16.68261	-0.67249	0.00653	4.5	9.1
55.0	-17.31061	-0.61073	0.00763	5.2	10.8
65.0	-17.85307	-0.54839	0.00864	6.7	12.9
75.0	-18.35938	-0.48065	0.00952	9.1	15.5
85.0	-18.65002	-0.45863	0.01009	10.6	16.5
95.0	-18.59678	-0.51740	0.01026	8.3	14.1
110.0	-18.40481	-0.62280	0.01023	5.3	10.1
130.0	-18.31359	-0.70229	0.01017	4.2	7.4
150.0	-18.31056	-0.73909	0.01014	4.4	6.6
170.0	-18.31906	-0.75424	0.01013	4.6	6.3

Source Energy: 5.5 MeV

Angle (deg)	Coefficient a	Coefficient b	Coefficient c	Av. MAD (%)	Max. Dev. (%)
0.5	-8.50918	-0.99050	0.00311	0.4	-0.6
1.5	-9.74493	-0.96953	0.00305	1.2	1.6
2.5	-10.37903	-0.95256	0.00304	1.8	2.4
4.0	-11.02157	-0.93180	0.00306	2.4	3.3
6.0	-11.64070	-0.91026	0.00312	3.0	4.0
8.5	-12.24270	-0.88884	0.00322	3.4	4.5
12.5	-13.01883	-0.85984	0.00345	3.8	4.9
17.5	-13.80868	-0.82813	0.00382	4.1	5.7
25.0	-14.76568	-0.78194	0.00450	4.4	6.8
35.0	-15.74444	-0.72261	0.00554	4.9	8.5
45.0	-16.51249	-0.66413	0.00662	5.4	9.8
55.0	-17.14815	-0.60454	0.00769	6.3	11.4
65.0	-17.67830	-0.54866	0.00867	7.5	13.3
75.0	-18.14754	-0.49304	0.00953	9.6	15.4
85.0	-18.41481	-0.47923	0.01010	10.5	15.9
95.0	-18.37967	-0.53582	0.01029	8.1	13.7
110.0	-18.18616	-0.64571	0.01026	4.7	9.3
130.0	-18.07745	-0.73343	0.01018	3.0	6.3
150.0	-18.06301	-0.77505	0.01014	3.1	5.1
170.0	-18.06879	-0.79191	0.01012	3.2	4.8

Source Energy: 4.5 MeV

Angle (deg)	Coefficient a	Coefficient b	Coefficient c	Av. MAD (%)	Max. Dev. (%)
0.5	-8.35440	-0.99054	0.00342	0.4	0.6
1.5	-9.57970	-0.96997	0.00335	1.2	1.7
2.5	-10.20947	-0.95221	0.00333	1.8	2.5
4.0	-10.84418	-0.93049	0.00334	2.5	3.4
6.0	-11.45245	-0.90776	0.00339	3.1	4.3
8.5	-12.04056	-0.88515	0.00349	3.7	4.9
12.5	-12.79416	-0.85529	0.00371	4.2	5.5
17.5	-13.56468	-0.82298	0.00406	4.6	6.0
25.0	-14.51023	-0.77656	0.00471	5.0	7.3
35.0	-15.49461	-0.71747	0.00570	5.7	9.0
45.0	-16.27127	-0.66035	0.00675	6.4	10.5
55.0	-16.90625	-0.60506	0.00777	7.3	12.0
65.0	-17.42659	-0.55583	0.00871	8.4	13.5
75.0	-17.85917	-0.51282	0.00954	10.0	15.0
85.0	-18.11836	-0.50407	0.01011	10.4	15.3
95.0	-18.11672	-0.55524	0.01034	8.0	13.2
110.0	-17.92974	-0.66827	0.01033	4.1	8.6
130.0	-17.78767	-0.76929	0.01022	1.6	5.0
150.0	-17.75403	-0.81884	0.01016	1.2	3.4
170.0	-17.75121	-0.83932	0.01013	1.3	2.8

Source Energy: 3.5 MeV

Angle (deg)	Coefficient a	Coefficient b	Coefficient c	Av. MAD (%)	Max. Dev. (%)
0.5	-8.17183	-0.98828	0.00389	0.5	1.1
1.5	-9.40385	-0.96308	0.00381	1.5	2.5
2.5	-10.03899	-0.94159	0.00379	2.2	3.8
4.0	-10.67691	-0.91572	0.00380	3.0	5.2
6.0	-11.28263	-0.88915	0.00385	3.7	6.4
8.5	-11.86211	-0.86334	0.00394	4.3	7.4
12.5	-12.59264	-0.83133	0.00414	4.9	8.4
17.5	-13.34028	-0.79744	0.00447	5.4	9.0
25.0	-14.26622	-0.75042	0.00508	5.9	9.6
35.0	-15.24439	-0.69262	0.00601	6.6	10.4
45.0	-16.02860	-0.63648	0.00700	7.4	11.8
55.0	-16.66515	-0.58478	0.00797	8.2	13.2
65.0	-17.17563	-0.54200	0.00887	9.1	14.5
75.0	-17.59695	-0.50551	0.00967	10.2	16.7
85.0	-17.85195	-0.50092	0.01025	10.3	17.0
95.0	-17.84378	-0.55745	0.01050	7.8	13.4
110.0	-17.58929	-0.69379	0.01046	4.0	8.0
130.0	-17.38142	-0.81832	0.01031	3.2	-5.1
150.0	-17.32045	-0.87894	0.01022	2.5	-6.3
170.0	-17.30779	-0.90388	0.01019	2.4	-6.4

Source Energy: 2.5 MeV

Angle (deg)	Coefficient a	Coefficient b	Coefficient c	Av. MAD (%)	Max. Dev. (%)
0.5	-7.92954	-0.98676	0.00464	0.6	1.7
1.5	-9.15743	-0.95848	0.00453	1.8	3.3
2.5	-9.79689	-0.93304	0.00450	2.7	5.1
4.0	-10.43662	-0.90238	0.00450	3.6	7.0
6.0	-11.03843	-0.87135	0.00454	4.5	8.8
8.5	-11.60502	-0.84194	0.00463	5.1	10.3
12.5	-12.31311	-0.80576	0.00481	5.8	11.8
17.5	-13.02839	-0.76978	0.00511	6.4	12.9
25.0	-13.91068	-0.72439	0.00565	7.0	13.9
35.0	-14.85561	-0.67139	0.00649	7.8	15.1
45.0	-15.62706	-0.61920	0.00740	8.6	16.5
55.0	-16.23975	-0.57630	0.00829	9.3	17.8
65.0	-16.73064	-0.54145	0.00913	9.9	19.2
75.0	-17.12407	-0.51501	0.00987	10.4	20.6
85.0	-17.37571	-0.51354	0.01045	10.2	20.3
95.0	-17.41302	-0.56089	0.01077	7.7	14.9
110.0	-17.13507	-0.70903	0.01078	6.3	-10.4
130.0	-16.80073	-0.87415	0.01058	8.7	16.3
150.0	-16.64530	-0.96460	0.01044	9.9	17.5
170.0	-16.59248	-1.00247	0.01038	10.2	-17.8

Source Energy: 1.5 MeV

Angle (deg)	Coefficient a	Coefficient b	Coefficient c	Av. MAD (%)	Max. Dev. (%)
0.5	-7.58567	-0.98475	0.00605	0.9	2.8
1.5	-8.81580	-0.94930	0.00590	2.6	4.9
2.5	-9.47027	-0.91570	0.00586	4.0	7.7
4.0	-10.12112	-0.87592	0.00585	5.3	10.9
6.0	-10.72606	-0.83646	0.00588	6.4	13.7
8.5	-11.28246	-0.80051	0.00594	7.3	16.2
12.5	-11.95995	-0.75838	0.00609	8.1	18.6
17.5	-12.62827	-0.71931	0.00634	8.8	20.4
25.0	-13.43664	-0.67503	0.00678	9.4	22.4
35.0	-14.30309	-0.62950	0.00748	10.0	24.0
45.0	-14.99557	-0.59361	0.00823	10.5	25.1
55.0	-15.54272	-0.56631	0.00899	10.7	25.8
65.0	-15.97945	-0.54493	0.00971	10.9	26.5
75.0	-16.32359	-0.53037	0.01037	11.1	27.2
85.0	-16.58714	-0.52369	0.01095	10.8	27.3
95.0	-16.72687	-0.54101	0.01139	9.4	24.6
110.0	-16.64413	-0.63341	0.01169	9.5	13.2
130.0	-16.23381	-0.81927	0.01160	15.5	34.6
150.0	-15.88589	-0.96327	0.01142	23.0	47.5
170.0	-15.71597	-1.03426	0.01132	25.9	52.2

Source Energy: 0.75 MeV

Angle (deg)	Coefficient a	Coefficient b	Coefficient c	Av. MAD (%)	Max. Dev. (%)
0.5	-7.14444	-0.99694	0.00839	1.0	2.3
1.5	-8.40557	-0.94672	0.00815	3.8	7.5
2.5	-9.08480	-0.90034	0.00808	5.6	10.7
4.0	-9.75001	-0.84825	0.00805	7.4	15.6
6.0	-10.35795	-0.79770	0.00806	8.9	20.2
8.5	-10.90872	-0.75179	0.00811	10.0	24.1
12.5	-11.55655	-0.70042	0.00822	11.0	28.1
17.5	-12.17259	-0.65601	0.00840	11.8	31.0
25.0	-12.87772	-0.61438	0.00872	12.5	33.5
35.0	-13.61158	-0.58111	0.00921	12.8	35.0
45.0	-14.18642	-0.56337	0.00974	12.9	35.4
55.0	-14.63111	-0.55635	0.01029	12.9	35.3
65.0	-14.97583	-0.55384	0.01085	12.9	35.1
75.0	-15.24170	-0.55479	0.01136	12.6	34.5
85.0	-15.46310	-0.55269	0.01186	12.4	34.2
95.0	-15.64410	-0.55038	0.01230	12.4	34.2
110.0	-15.85622	-0.54637	0.01287	12.2	34.1
130.0	-16.06595	-0.53718	0.01350	12.2	34.4
150.0	-16.20228	-0.52879	0.01393	12.2	34.6
170.0	-16.26594	-0.52541	0.01413	12.2	34.7

Source Energy: 0.325 MeV

Angle (deg)	Coefficient a	Coefficient b	Coefficient c	Av. MAD (%)	Max. Dev. (%)
0.5	-6.71592	-1.03172	0.01153	1.6	3.3
1.5	-8.07690	-0.94581	0.01120	5.8	13.0
2.5	-8.78940	-0.88085	0.01112	8.4	17.3
4.0	-9.47427	-0.81217	0.01108	10.9	21.8
6.0	-10.09263	-0.74702	0.01108	12.7	28.4
8.5	-10.63353	-0.69058	0.01111	14.2	34.3
12.5	-11.25494	-0.62881	0.01120	15.5	40.0
17.5	-11.82104	-0.57826	0.01133	16.3	44.2
25.0	-12.43931	-0.53484	0.01155	16.9	47.3
35.0	-13.03722	-0.51037	0.01186	16.9	48.6
45.0	-13.48116	-0.50724	0.01218	16.5	47.8
55.0	-13.80129	-0.51925	0.01251	15.9	45.9
65.0	-14.03747	-0.53675	0.01287	15.2	43.5
75.0	-14.21578	-0.55331	0.01323	14.4	40.9
85.0	-14.35568	-0.56531	0.01359	13.8	38.7
95.0	-14.46665	-0.57279	0.01391	13.2	37.0
110.0	-14.60595	-0.57434	0.01434	12.6	35.2
130.0	-14.74812	-0.56676	0.01483	12.2	34.1
150.0	-14.84392	-0.55716	0.01517	11.9	33.7
170.0	-14.89213	-0.55091	0.01535	11.8	33.8

Source Energy: 0.1 MeV

Angle (deg)	Coefficient a	Coefficient b	Coefficient c	Av. MAD (%)	Max. Dev. (%)
0.5	-6.40158	-1.04235	0.01675	2.1	4.5
1.5	-7.81309	-0.92558	0.01632	6.8	14.6
2.5	-8.50949	-0.85097	0.01622	9.5	18.9
4.0	-9.16255	-0.77588	0.01617	11.8	25.0
6.0	-9.73855	-0.70714	0.01617	13.5	31.6
8.5	-10.23417	-0.64890	0.01621	14.8	36.8
12.5	-10.78308	-0.58847	0.01631	15.8	41.6
17.5	-11.25874	-0.54288	0.01643	16.3	44.6
25.0	-11.74978	-0.50890	0.01663	16.4	46.2
35.0	-12.18135	-0.50036	0.01687	16.0	45.5
45.0	-12.47044	-0.51439	0.01710	15.2	43.1
55.0	-12.66152	-0.54219	0.01734	14.2	39.8
65.0	-12.78589	-0.57551	0.01758	13.1	36.0
75.0	-12.86513	-0.60814	0.01784	11.9	32.0
85.0	-12.91613	-0.63496	0.01810	10.9	28.4
95.0	-12.95385	-0.65299	0.01835	9.9	25.5
110.0	-13.00502	-0.66188	0.01874	8.9	22.5
130.0	-13.06711	-0.65253	0.01923	8.1	21.1
150.0	-13.10413	-0.64177	0.01957	7.7	20.3
170.0	-13.12132	-0.63549	0.01974	7.5	19.9

APPENDIX B

Gamma-Ray Mass Interaction Coefficients

Gamma-ray mass interaction coefficients (total - coherent scattering) used in the *MicroSkyshine* program and in the generation of line-beam response functions. Data for Zr are from the report of Storm and Israel [St67] All other data are from the compilation of Hubbell [Hu82].

E (MeV)	μ/ρ (cm^2/g)						
	Air	H2O	Concrete	Fe	Pb	Zr	UO_2
0.10	0.15410	0.17070	0.17810	0.37010	5.55000	0.91100	1.74100
0.15	0.13560	0.15040	0.14330	0.19600	2.01400	0.35300	2.30000
0.20	0.12340	0.13700	0.12700	0.14580	0.99850	0.20800	1.15900
0.30	0.10680	0.11870	0.10820	0.10980	0.40260	0.12300	0.47030
0.40	0.09548	0.10610	0.09629	0.09398	0.23230	0.09700	0.26890
0.50	0.08712	0.09687	0.08767	0.08413	0.16130	0.08450	0.18450
0.60	0.08056	0.08957	0.08098	0.07703	0.12480	0.07530	0.14090
0.80	0.07075	0.07866	0.07103	0.06698	0.08869	0.06450	0.09796
1.00	0.06359	0.07070	0.06381	0.05994	0.07103	0.05720	0.07713
1.50	0.05176	0.05755	0.05197	0.04883	0.05222	0.04650	0.05539
2.00	0.04447	0.04940	0.04482	0.04265	0.04607	0.04120	0.04826
3.00	0.03581	0.03969	0.03654	0.03622	0.04234	0.03620	0.04345
4.00	0.03079	0.03403	0.03189	0.03311	0.04197	0.03470	0.04238
5.00	0.02751	0.03031	0.02895	0.03146	0.04272	0.03400	0.04263
6.00	0.02523	0.02771	0.02696	0.03057	0.04391	0.03390	0.04342
8.00	0.02225	0.02429	0.02450	0.02991	0.04675	0.03410	0.04569
10.00	0.02045	0.02219	0.02311	0.02994	0.04972	0.03520	0.04826

APPENDIX C

Coefficients for Air-Kerma (Exposure) Buildup Factors

Coefficients for the geometric-progression form [Ha83, Ha86] of air-kerma (exposure) buildup factors as reported in the QAD-CGCP program [Rs86] and as used in the generation of line-beam response functions.

E(MeV)	b	c	a	X_k	d
0.015	1.170	0.459	0.175	13.73	-0.0862
0.020	1.407	0.512	0.161	14.40	-0.0819
0.030	2.292	0.693	0.102	13.34	-0.0484
0.040	3.390	1.052	-0.004	19.76	-0.0068
0.050	4.322	1.383	-0.071	13.51	0.0270
0.060	4.837	1.653	-0.115	13.66	0.0511
0.080	4.929	1.983	-0.159	13.74	0.0730
0.100	4.580	2.146	-0.178	12.83	0.0759
0.150	3.894	2.148	-0.173	14.46	0.0698
0.200	3.345	2.147	-0.176	14.08	0.0719
0.300	2.887	1.990	-0.160	14.13	0.0633
0.400	2.635	1.860	-0.146	14.24	0.0583
0.500	2.496	1.736	-0.130	14.32	0.0505
0.600	2.371	1.656	-0.120	14.27	0.0472
0.800	2.207	1.532	-0.103	14.12	0.0425
1.000	2.102	1.428	-0.086	14.35	0.0344
1.500	1.939	1.265	-0.057	14.24	0.0232
2.000	1.835	1.173	-0.039	14.07	0.0161
3.000	1.712	1.051	-0.011	13.67	0.0024
4.000	1.627	0.983	0.006	13.51	-0.0051
5.000	1.558	0.943	0.017	13.82	-0.0117
6.000	1.505	0.915	0.025	16.37	-0.0231
8.000	1.418	0.891	0.032	12.06	-0.0167
10.000	1.358	0.875	0.037	14.01	-0.0226
15.000	1.267	0.844	0.048	14.55	-0.0344